EFFECTS OF GROUND PROFILE ON THE PERFORMANCE OF AIR TRAFFIC CONTROL RADAR BEACON SYSTEMS

Chiao-Min Chu
Dipak L. Sengupta

Abstract

Theoretical expressions necessary to obtain the effects of ground profile on the SLS mode performance of an ATCRBS have been derived. The theory is based on ray optics and neglects any effects of diffraction. Focussing effects of ordinary concave cylindrical surfaces are found to be important in regions very close to the horizon. It is believed that such effects will not be of significance for normal ATCRBS operation.

On the basis of the theoretical formulations a computer program has been developed to obtain numerical results for ATCRBS using various antenna systems located above a ground with a specified profile. It is assumed that the ground consists of planar sections having arbitrary dielectric constant. The computer program is capable of handling any ground profile as long as it can be approximated by planar sections. Some representative results are discussed for simple cases of a ground consisting of two planar sections. The performance of an ATCRBS located at the NAFEC area has been studied theoretically by assuming a ground profile typical of the NAFEC area. Theoretical results are compared with those obtained in actual flight tests.

Key words:

SLS mode performance of ATCRBS
Effects of ground profile
Computer program for ATCRBS performance
Caustic effects on ATCRBS performance
Theoretical and flight test results at NAFEC

MISSING PAGE

PREFACE

The report investigates theoretically the effects of ground profile on the SLS mode performance of an ATCRBS. A computer program is developed to obtain numerical results for the various quantities characterizing the performance of ATCRBS located above a ground of given profile and having arbitrary dielectric constant. The program can handle any ground profile as long as it can be approximated by linear sections. Diffraction effects are neglected. The computer program has been prepared by G. F. Hopp.

MISSING PAGE

TABLE OF CONTENTS

LIST OF ILLUSTRATIONS

List of Illustrations (cont'd)

List of Illustrations

LIST OF TABLES

1. INTRODUCTION

The overall performance of Air Traffic Control Radar Beacon System (ATCRBS) using various interrogator antenna systems located above a perfectly dielectric flat ground has been discussed theoretically in our earlier reports [1, 2]. In the present report an attempt is made to develop analytical and computational techniques by which the ATCRBS performance may be quantitatively assessed when the ground is of a given profile. For simplicity of analysis the variations in the ground surface are assumed to be two dimensional; in spite of this restriction, it is believed that the results of the present investigation may find applications in many practical situations. The main task involved in the present study can be stated as follows: given the free space far field patterns of the interrogator antenna system, obtain the modification of its far zone field patterns when the antenna system is placed above a ground with known electrical properties and a given profile in the vertical plane. From a knowledge of the modified field patterns, it is possible to obtain the various quantities characterizing the performance of an ATCRBS in the presence of the assumed ground. Only the SLS mode performance of ATCRBS is considered in the present report. For a given antenna system the following quantities of interest characterizing the ATCRBS performance are studied: P1 and P2 pulse amplitude patterns, P1/P2 pulse ratio patterns, the effective azimuth beamwidth, and the number of replies.

The outline of the report is as follows. Section 2 discusses the theoretical approach to obtain the effects of ground profile on the radiation pattern of a given antenna. Profiles of ground consisting of planar surfaces and the effects of reflections from convex and concave surfaces are considered. For realistic ground profiles the numerical method is the most convenient way of obtaining meaningful results. Section 3 uses the ideas and results of Section 2 to develop a general computer program for calculating the various quantities characterizing the performance of ATCRBS in the presence of a ground whose profile may be approximated by sections of planar sections. The effects of diffraction, multiple reflection and the curvature of the ground are neglected. If necessary, these effects may be included in the program. The computer program is developed such that the output data and format correspond to the general

ATCRBS computer program discussed in our previous reports [1, 2]. Section 4 discusses some simple numerical examples to illustrate the power and the capabilities of the computer program. Numerical results are obtained for an ATCRBS using the Hazeltine open array antenna system [1]. Theoretical results are also obtained for this ATCRBS in the presence of an assumed ground profile which approximates a typical terrain profile in the NAFEC area as seen by an aircraft during a radial flight at constant height. Theoretical results are compared with those obtained by actual flight tests. Some numerical results are also obtained for the P1 pulse amplitude patterns for an ATCRBS using the existing Hog-Trough antenna [1] located above a selected NAFEC ground profile. Measured results for this case are not available at the present time.

2. EFFECTS OF GROUND PROFILE ON RADIATION PATTERN

2.1 General Statement of the Problem

Given the free space far field pattern of an antenna, we are interested in investigating the modification of the far zone field pattern when the antenna is placed above a ground with known complex dielectric constant (or index of refraction) and a given profile. We shall carry out our investigation based on the following conditions:

a) Assume the antenna is vertically polarized, and the free space far field pattern $f(\theta, \phi)$ is known. To conform with the notation used in our previous work, the elevation angle θ is measured from the horizontal, as illustrated in Fig. 1.

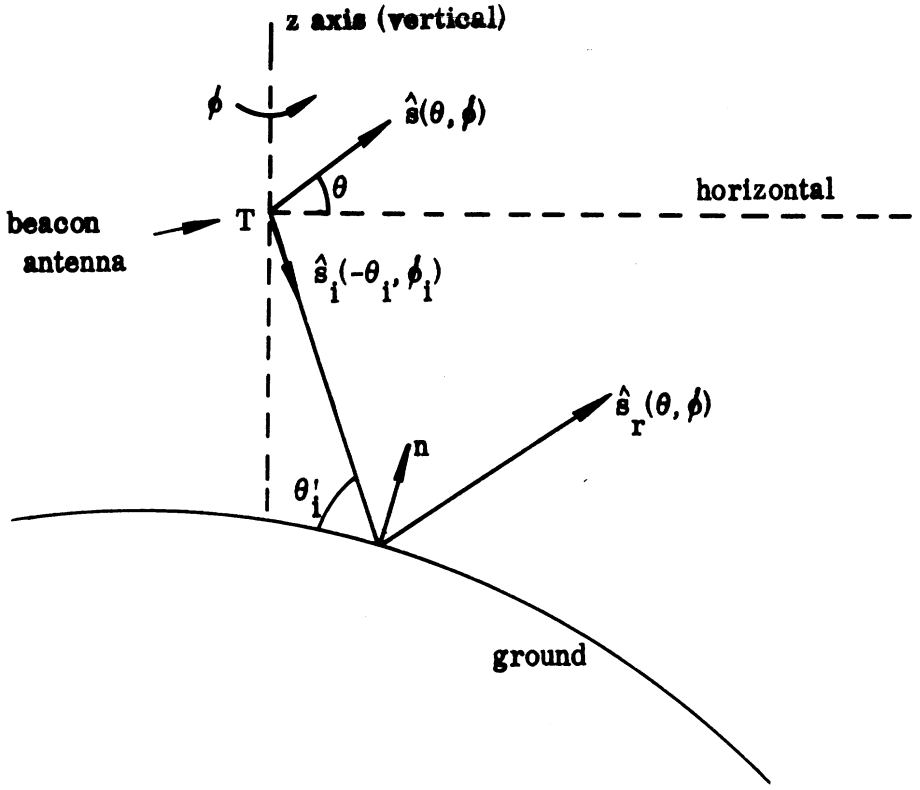

FIG. 1: The geometry of the problem.

b) Assume that the ground profile is smooth (with very small slope), and that as a first approximation, the geometrical optics approach is valid. Moreover, the reflected wave from the ground may be assumed to be essentially vertically polarized.

c) We are interested primarily in the far field pattern at small elevation angles.

To study the effect of ground profile, let us refer to Fig. 1 and consider an incident ray in the direction of the unit vector $\hat{s}_i(-\theta_i, \phi_i)$. When this ray is reflected from the ground, the direction of the reflected ray is given by $\hat{s}_r(\theta, \phi)$. If the unit normal, $\hat{n}$, to the ground at the reflection point is known, then the reflected direction is given by

$$\hat{s}_r(\theta, \phi) = \hat{s}_i(\theta_i, \phi_i) - 2(\hat{s}_i \cdot \hat{n})\,\hat{n} \quad . \tag{1}$$

Assuming that for smooth ground, multiple reflection does not occur, then this reflected ray would interfere in the far zone with a direct ray in the direction $\hat{s}(\theta, \phi)$ and modify the field pattern. In general, given a direction (θ, ϕ), and depending on the ground profile, there may be several incident directions $(-\theta_i, \phi_i)$ that would reflect in the direction (θ, ϕ). (See, for example, Section 2.2). It appears, therefore, that the first problem to be solved is: Given any direction (θ, ϕ) and a given ground profile, find all the values (θ_i, ϕ_i) satisfying Eq. (1). Although in principle a computer program may be developed to solve this problem (discussed in Section 2.2), in the present chapter we assume that the smooth ground profile may be approximated in sections by inclined planes, and by concave or convex quadratic surfaces, and derive appropriate analytic expressions for computation later.

To calculate quantitatively the modification of the field pattern, it is necessary to know the reflected field in the far zone region. To obtain the reflected field, it is necessary to know the following quantities:

(i) The reflection coefficient [3],

$$\rho = \frac{N^2 \sin\theta_i' - \sqrt{N^2 - 1 + \sin^2\theta_i'}}{N^2 \sin\theta_i' + \sqrt{N^2 - 1 + \sin^2\theta_i'}} \tag{2}$$

where

$$N = \sqrt{\epsilon_r - \frac{j\sigma}{\omega\epsilon_0}} \tag{3}$$

is the index of refraction of the ground, and θ_i' is the angle between the incident ray and the tangent plane at the point of reflection, i.e.,

$$\sin\theta_i' = -\hat{n}\cdot\hat{s}_i = \hat{n}\cdot\hat{s}_r \quad . \tag{4}$$

(ii) The divergence factor D due to the curvature of the ground profile, which may be approximately calculated (see Appendix A).

(iii) The path difference Δ between the direct ray and the reflected ray, which may be calculated if the ground profile is known.

Incorporation the three factors ρ, Δ, D above, the combined far zone field at a point (R,θ,ϕ) due to the direct and the reflected rays are given by

$$E(\theta,\phi) = \frac{\sqrt{30\ WG}}{R}\ e^{-j\beta R}\left\{f(\theta,\phi)+\sum\rho D f(-\theta_i,\phi_i)\, e^{-j\beta\Delta}\right\} \tag{5}$$

where the summation is over all possible directions $(-\theta_i,\phi_i)$ corresponding to the reflected direction $\hat{s}(\theta,\phi)$, and ρ, D, Δ are all functions of θ_i, ϕ_i, W is the effective radiated power and G is the gain of the antenna.

In the present section we investigate the effects of simple ground profiles, such as plane, convex and concave cylindrical surfaces on the reflected rays and use these results later to "synthesize" the reflected field of a realistic "smooth" ground profile.

2.2 Planar Profiles

In this section we consider, as a first approximation, the reflection from a ground whose profile may be approximated by sections of planar surfaces, as illustrated in Fig. 2. Neglecting the diffracted field at the corners, the reflection from each planar section may be considered separately. For example, the section AB of the ground profile in Fig. 2 may be considered as part of a large ground plane as illustrated in Fig. 3. If the normal to AB is inclined at an angle α to the vertical (z-axis) and has an azimuth angle β related to an arbitrarily chosen x-axis, then we have

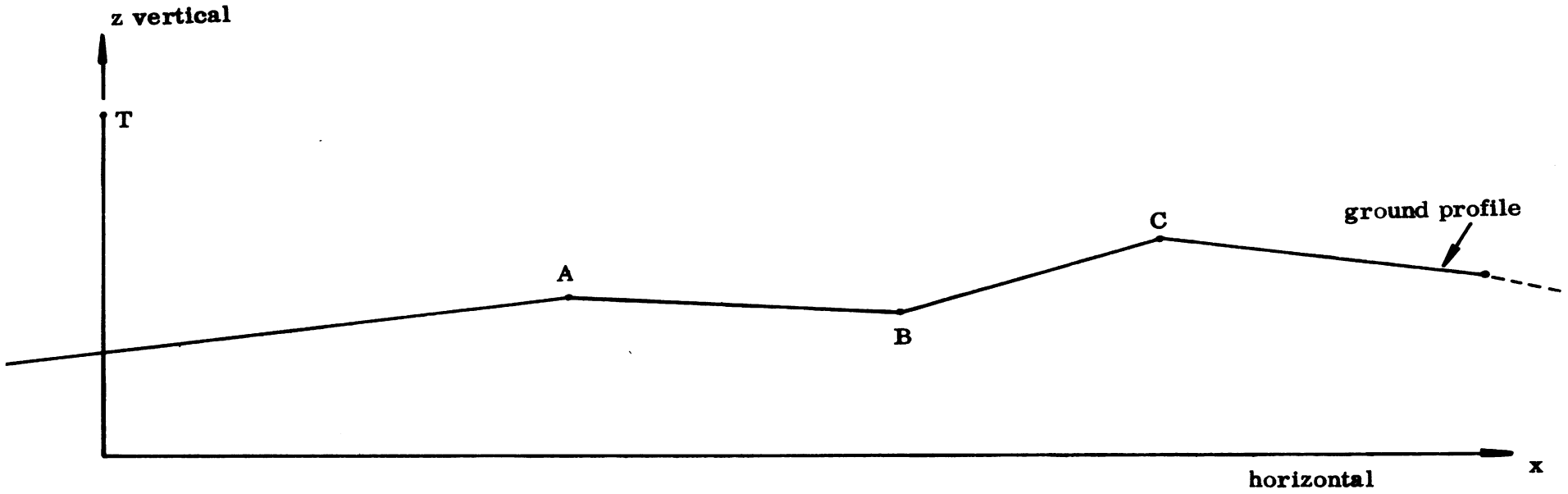

FIG. 2: Ground profile consisting of a number of linear sections.

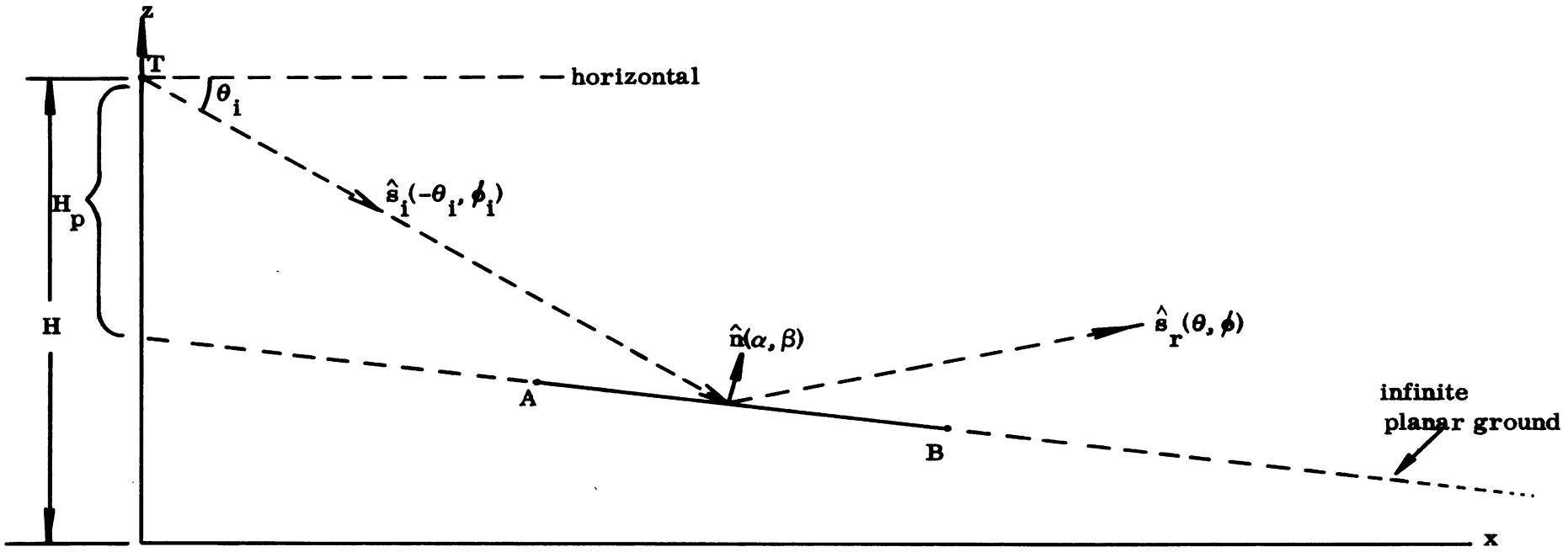

FIG. 3: Section AB of Fig. 2 may be considered as a part of a large inclined plane.

$$\hat{n}(\alpha,\beta) = \hat{z}\cos\alpha + \hat{x}\sin\alpha\cos\beta + \hat{y}\sin\alpha\sin\beta \ . \tag{6}$$

From Eqs. (1) and (6), the following relations may be obtained.

a) Reflected direction in terms of incident direction:

$$\sin\theta = \sin\theta_i\cos 2\alpha - \sin 2\alpha\cos\theta_i\cos(\phi_i - \beta) \tag{7}$$

$$\cos\theta\begin{Bmatrix}\cos\phi\\ \sin\phi\end{Bmatrix} = \cos\theta_i\begin{Bmatrix}\cos\phi_i\\ \sin\phi_i\end{Bmatrix} + \sin 2\alpha\sin\theta_i\begin{Bmatrix}\cos\beta\\ \sin\beta\end{Bmatrix}$$

$$-(1-\cos 2\alpha)\cos(\phi_i - \beta)\cos\theta_i\begin{Bmatrix}\cos\beta\\ \sin\beta\end{Bmatrix} \tag{8}$$

The two equations in Eq. (8) determine ϕ without ambiguity.

b) Incident direction in terms of reflected direction:

$$\sin\theta_i = \sin\theta\cos 2\alpha + \sin 2\alpha\cos\theta\cos(\phi - \beta) \tag{9}$$

$$\cos\theta_i\begin{Bmatrix}\cos\phi_i\\ \sin\phi_i\end{Bmatrix} = \cos\theta\begin{Bmatrix}\cos\phi\\ \sin\phi\end{Bmatrix} - \sin 2\alpha\sin\theta_i\begin{Bmatrix}\cos\beta\\ \sin\beta\end{Bmatrix}$$

$$-(1-\cos 2\alpha)\cos(\phi - \beta)\cos\theta\begin{Bmatrix}\cos\beta\\ \sin\beta\end{Bmatrix} \tag{10}$$

Comments similar to Eq. (8) apply to Eq. (10) also.

c) The "angle of incidence" θ_i':

$$\sin\theta_i' = \cos\alpha\sin\theta_i - \sin\alpha\cos\theta_i\cos(\phi_i - \beta) = \cos\alpha\sin\theta + \sin\alpha\cos\theta\cos(\phi - \beta) \tag{11}$$

The above equations enable one to determine the direction of the reflected field, and the reflection coefficient ρ. For planar sections, the divergence factor D is unity, so that in order to compute the reflected field, we need the path differences Δ. From geometrical configurations, it is easily seen that

$$\Delta = 2H_p \cos\alpha \left[\cos\alpha \sin\theta + \sin\alpha \cos\theta \cos(\phi - \beta)\right] , \tag{12}$$

where H_p is as shown in Fig. 3.

Although the above equations are useful in detailed numerical computation of the reflected fields, we shall at present consider a simple case when $\beta = 0$. Moreover, since the x-direction may be arbitrarily chosen, we shall assume that $\phi_i = 0$. For this case, the above equations may be simplified to

$$\phi = 0 \tag{13}$$

$$\theta_i = \theta + 2\alpha \tag{14a}$$

or

$$\theta = \theta_i - 2\alpha \tag{14b}$$

$$\theta_i' = \theta_i - \alpha = \theta + \alpha \tag{15}$$

and

$$\Delta = 2H_p \cos\alpha \sin(\theta + \alpha) \tag{16}$$

Let us now apply the above equations to a hypothetical ground profile consisting of three planar sections, I, II and III, as illustrated in Fig. 4. For simplicity, we choose the profile such that every portion of the ground is illuminated (no shadowing), and all the reflected rays reach the far zone and interfere with the direct ray (no multiple reflection). As illustrated in Fig. 4, the planar section I starts at the point $C(x_c, z_c)$ with a downward slope $\tan\alpha_1$ and is illuminated by rays with incident direction

$$\theta_c \geq \theta_i \geq \alpha_1$$

where

$$\theta_c = \tan^{-1} \frac{H - z_c}{x_c} \tag{17}$$

and H is the height of the antenna. The planar section II is between $B(x_b, z_b)$ and $C(x_c, z_c)$, and has an upward slope

$$\tan\alpha_2 = - \frac{z_c - z_b}{x_c - x_b} . \tag{18}$$

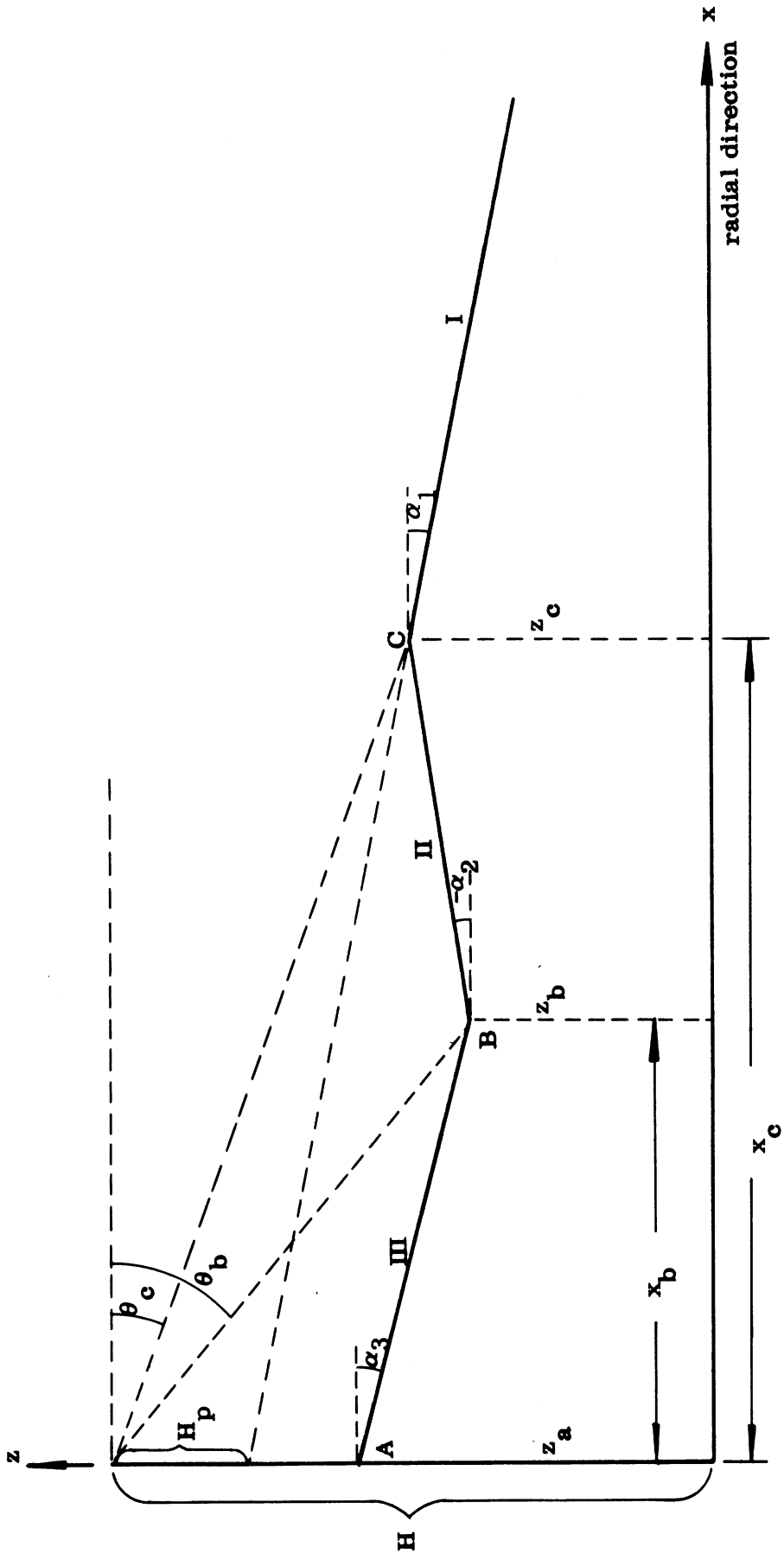

FIG. 4: Beacon antenna located above a ground profile consisting of three linear sections.

This section is illuminated by incident rays with incident direction

$$\theta_b \geq \theta_i \geq \theta_c \tag{19}$$

where
$$\theta_b = \tan^{-1} \frac{H - z_b}{x_b} \quad . \tag{20}$$

Similarly, the section III is between $A(\theta, z_a)$ and $B(x_b, z_b)$, and has a downward slope

$$\tan\alpha_3 = \frac{z_a - z_b}{x_b} \quad . \tag{21}$$

This section is illuminated by incident rays with incident direction

$$\theta_i \geq \theta_b \quad . \tag{22}$$

Using equations (13) to (16), we may construct a table for the directions of incidence and reflection, the angle of incidence, and the path difference for the rays reflected from each part of the ground. This is given in Table 1.

To interpret the information given in the table, and to use it to compute the reflected and total fields, let us plot θ_i, θ_i' and Δ against θ, as shown in the sketches given by Figs. 5, 6, and 7 respectively. From these figures, the following appear to be clear:

a) From Fig. 5, it is seen that in the range of θ from $-\alpha_1$ to $\theta_c - 2\alpha_1$, we have only one reflected ray, reflected from part I of the ground. Similarly for the range of θ from $\theta_c - 2\alpha_2$ to $\theta_b - 2\alpha_3$, we have only one reflected ray from part II of the ground while for the range of θ from $\theta_b - 2\alpha_2$ to 90^o, we have only one reflected ray from part III of the ground.

TABLE I

ANGLES OF INCIDENCE, REFLECTION AND THE PATH DIFFERENCE APPROPRIATE FOR VARIOUS GROUND SECTIONS

Ground Section	θ_i, incident direction	θ, reflected direction (Eq. 14)	θ_i', angle of incidence (Eq. 15)	Δ, path difference (Eq. 16)
I	$\theta_c \geq \theta_i \geq \alpha_1$	$\theta_c - 2\alpha_1 \geq \theta \geq -\alpha_1$	$\theta_c - \alpha_1 \geq \theta_i' \geq 0$	$[\cos\alpha_1 \sin(\theta+\alpha_1)] \times 2(H - z_c - x_c \tan\alpha_1)$
II	$\theta_b \geq \theta_i \geq \theta_c$	$\theta_b - 2\alpha_2 \geq \theta \geq \theta_c - 2\alpha_2$	$\theta_b - \alpha_2 \geq \theta_i' \geq \theta_c - \alpha_2$	$[\cos\alpha_2 \sin(\theta+\alpha_2)] \times 2(H - z_b - x_b \tan\alpha_2)$
III	$\theta_i \geq \theta_b$	$\theta \geq \theta_b - 2\alpha_3$	$\theta_i' \geq \theta_c - \alpha_3$	$[\cos\alpha_3 \sin(\theta+\alpha_3)] \times 2(H - z_a)$

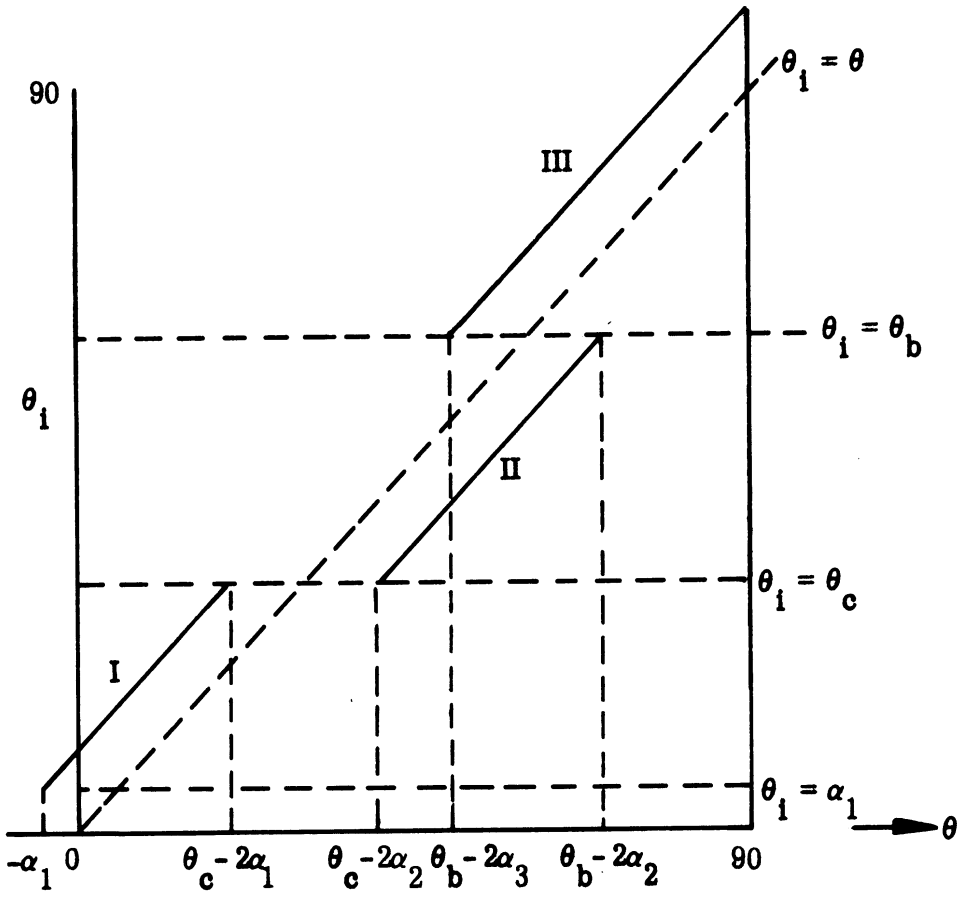

FIG. 5: Plot of θ_i vs. θ.

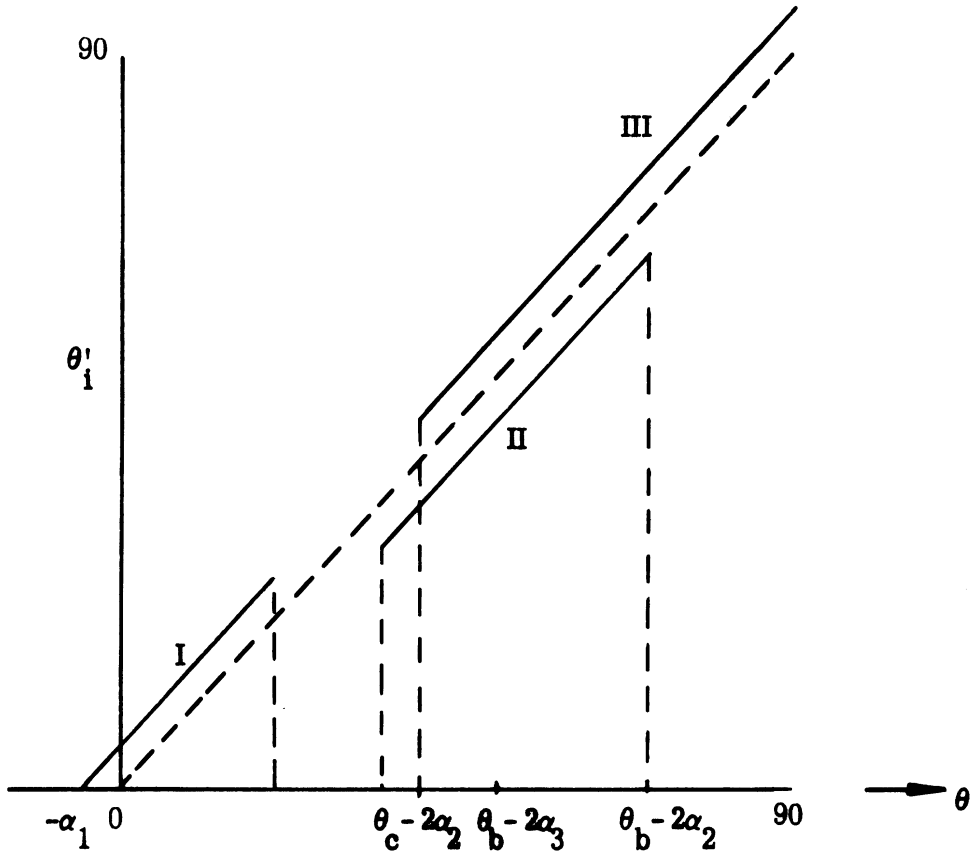

FIG. 6: Plot of θ'_i vs. θ.

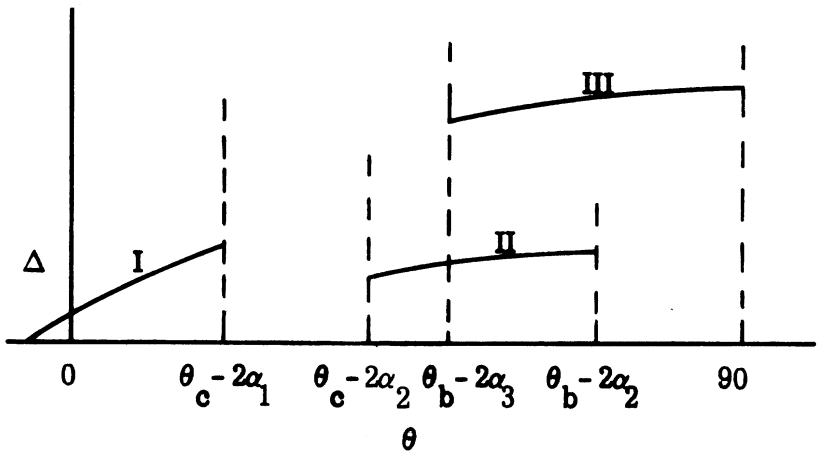

FIG. 7: Plot of the path difference Δ vs. θ.

b) From Fig. 5, it is seen that in the range of θ from $\theta_c - 2\alpha_1$ to $\theta_c - 2\alpha_2$, no reflected field is predicted by this approximate model. This is generally true if we approximate a convex surface by two planes and neglect the diffraction at the joint. An improved model taking into consideration the curvature at the transition to estimate the reflected field for convex surfaces is considered in Section 2.3.

c) In the range of θ from $\theta_c - 2\alpha_2$ to $\theta_b - 2\alpha_3$, we have two reflected rays, reflected from part II and part III of the composite ground. This is generally true if we approximate a concave surface by two planes. For concave surfaces with smooth transition, such as in the case of a cylindrical cavity, this piecewise planar approximation may not be accurate, and a detailed analysis is carried out in Section 2.3.

d) For each direction θ, knowing θ_i', the number of reflected rays, the path difference Δ for each ray, and the local properties of the ground, the total field can be computed from Eq. 5.

e) In the case of a vertically polarized antenna, and for small θ, we know $\rho = -1$. Then the information about Δ given in Fig. 7 for the case where there is only one reflected ray (such as part I of the curve) may be used approximately to estimate the first few minima of the total field pattern by finding θ_{min} such that

$$\beta\Delta(\theta_{min}) = 2n\pi \ , \qquad n = 1, 2, 3 \ldots \tag{23}$$

2.3 Reflection from Convex Surfaces

When a given ground profile cannot be approximated accurately by sections of planar surfaces, an improved model for the profile may be introduced by joining planar surfaces by quadratic surfaces to yield a smooth transition of the slope of the ground profile. For convex surfaces, such a model is illustrated in Fig. 8. In this figure, we show that two planar parts, I and III, are joined smoothly by part II. We shall assume that the planar part I has a downward sloping angle α_1, while the planar part III, starting from $A(0, z_a)$, has a downward sloping angle α_3. For simplicity, the smooth surface is assumed to be a circular cylinder with center at (x_0, z_0) and

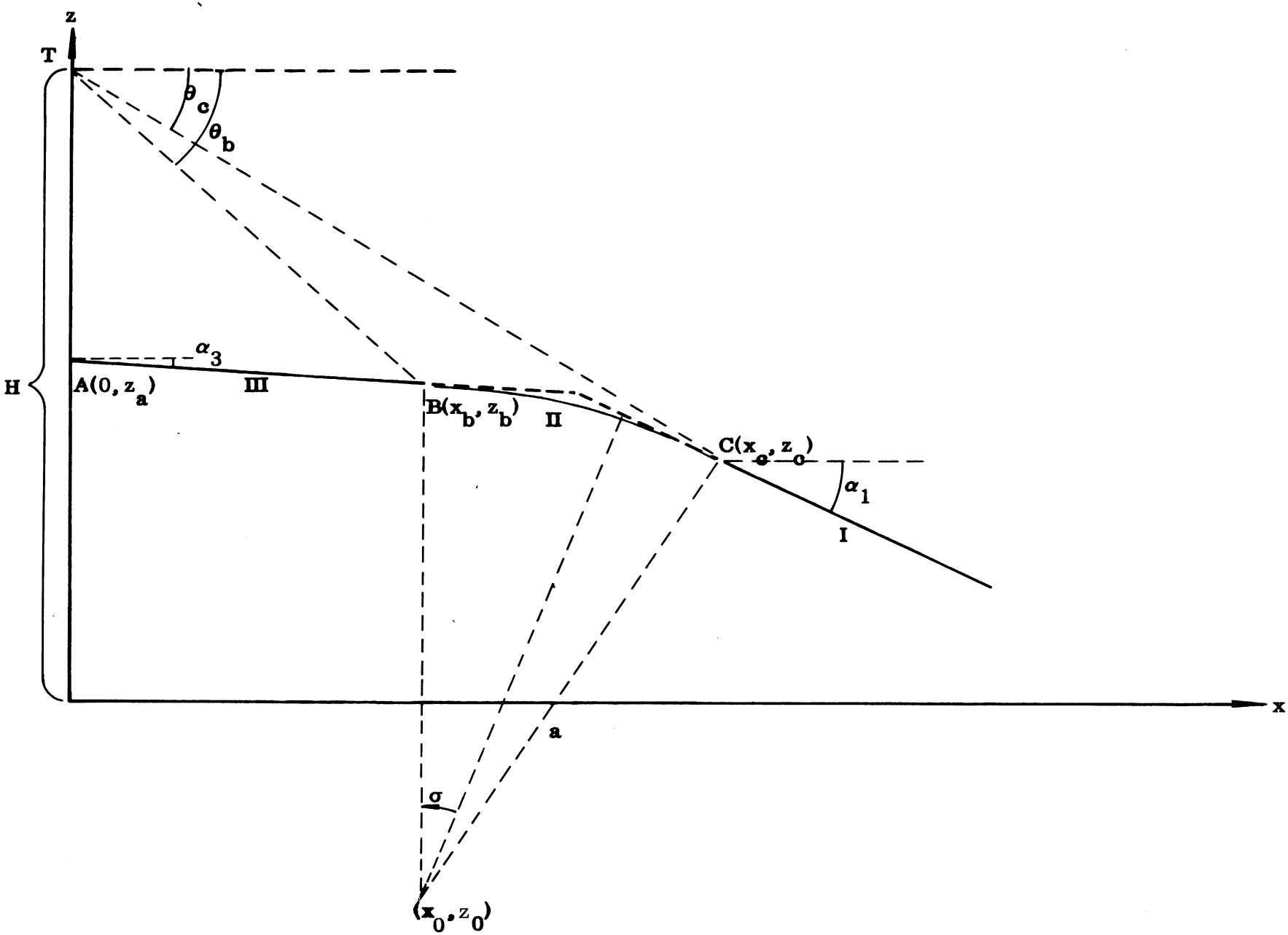

FIG. 8: Two planar sections smoothly joined by a convex section.

radius a. The points $B(x_b, z_b)$ and $C(x_c, z_c)$ where the planar surfaces join the cylinder are given respectively by

$$x_b = x_0 + a\sin\alpha_3 \quad , \qquad z_b = z_0 + a\cos\alpha_3 \tag{24}$$

and

$$x_c = x_0 + a\sin\alpha_1 \quad , \qquad z_c = z_0 + a\cos\alpha_1 \quad . \tag{25}$$

Any point on the cylindrical section BC can be represented in the parametric form

$$x = x_0 + a\sin\sigma \quad , \qquad z = z_0 + a\cos\sigma \tag{26}$$

where

$$\alpha_1 \geq \sigma \geq \alpha_3 \quad . \tag{27}$$

The reflected rays from this composite surface therefore consist of three types:

a) For $\theta_c \geq \theta_i \geq \alpha_1$,

where $$\theta_c = \tan^{-1}\frac{H - z_c}{x_c} \quad , \tag{28}$$

rays are reflected from part I of the surface. From the results of Section 2.2, we see that for each θ_i, the direction of the reflected ray is

$$\theta = \theta_i - 2\alpha_1 \quad , \tag{29}$$

the angle of incidence is

$$\theta_i' = \theta_i - \alpha_1 \quad , \tag{30}$$

and the path difference is

$$\Delta = 2(H - z_c - x_c\tan\alpha_1)\cos\alpha_1\sin(\theta + \alpha_1) \quad . \tag{31}$$

b) Similarly, for $\theta_i \geq \theta_b$,

where
$$\theta_b = \tan^{-1} \frac{H - z_b}{x_b} \quad , \tag{32}$$

rays are reflected from part III of the surface. For each θ_i, we have

$$\theta = \theta_i - 2\alpha_3 \tag{33}$$

$$\theta_i' = \theta_i - \alpha_3 \tag{34}$$

and
$$\Delta = 2(H - z_a)\cos\alpha_3 \sin(\theta + \alpha_3) \quad . \tag{35}$$

c) For $\theta_b \geq \theta \geq \theta_c$, the rays are reflected from a cylindrical surface of radius a. In Appendix A it is shown that, according to geometric optics, the rays reflected from such convex surfaces have the same direction and path difference as the rays reflected from the tangent plane. The amplitude of the field associated with the rays, however, has to be corrected by a "divergence factor" given by

$$D = \sqrt{\frac{a \sin\theta_i'}{2R_1 + a \sin\theta_i'}} \tag{36}$$

where θ_i' is the angle of incidence,

and R_1 is the distance from the antenna to the point of reflection.

Using the parametric form representing the cylindrical surface (Eqs. 26 and 27), we see that for given σ, the slope of the tangent plane is σ, and the incident angle is

$$\theta_i = \tan^{-1} \frac{H - z_0 - a\cos\sigma}{x_0 + a\sin\sigma} \quad . \tag{37}$$

Thus we have

$$\theta = \theta_i - 2\sigma \tag{38}$$

$$\theta_i' = (\theta_i - \sigma) \tag{39}$$

$$R_1 = \left[(H - z_0 - a\cos\sigma)^2 + (x_0 + a\sin\sigma)^2\right]^{1/2} \tag{40}$$

and

$$\Delta = 2(H - z_0 - a\sec\sigma - x_0\tan\sigma)\cos\theta\sin(\theta+\sigma) \quad . \tag{41}$$

Based on Eqs. (29), (33) and (38), we may sketch the θ_i, θ relations as shown in Fig. 9. From Fig. 9, we see that for each θ, there is only one reflected ray.

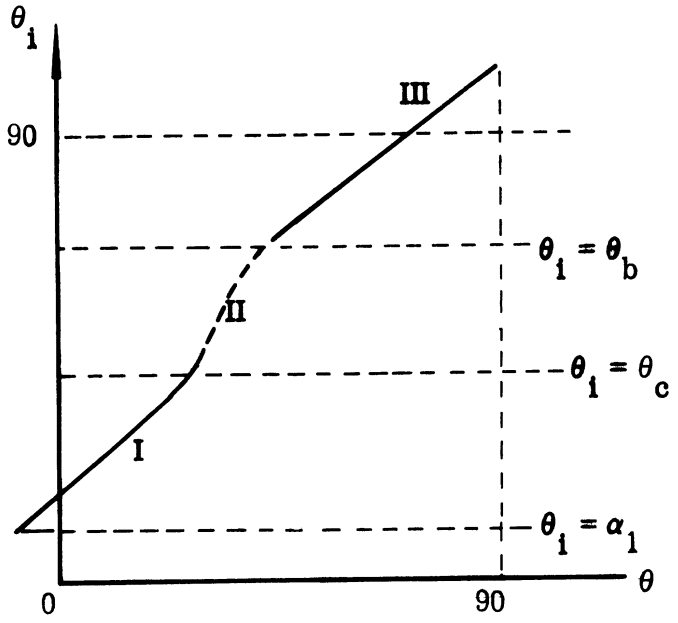

FIG. 9: θ_i vs. θ for the ground profile shown in Fig. 8.

These reflected rays may be computed by using the appropriate ρ, Δ and D, and combined with the direct ray to yield the far zone pattern.

It is to be noted that if the planar section III and I are extended and joined discontinuously (in slope) then, according to section 2.2, there would be a range of θ in which direction there are no reflected rays, if the diffraction fields are neglected. The "smooth" model introduced here, therefore, gives the first order correction for the neglected diffraction field. A more refined model may be obtained by using surfaces of continuous variation of radius of curvature so that the divergence factor D given by Eq. (36) does not change abruptly at points B and C.

2.4 Reflection from Concave Surfaces

In section 2.2, it is seen that if a ground profile is concave and is approximated by two planar surfaces joined together with a discontinuity in slope, there exists a range of reflected direction where one may observe more than one reflected ray. In general, for a concave surface with continuous slope variation, there exists a region where the reflected rays may converge and form a caustic. To simplify the analysis, we may represent part of a concave surface by a concave cylinder (with constant radius of curvature), and study the reflection from a concave cylinder. The reflection from any concave surface with varying radius of curvature can then be estimated by approximating the given surface with several sections of cylinders.

In Appendix A, the reflection of rays from a concave cylindrical surface are investigated. The results are summarized and illustrated in this section. Let us denote

a = the radius of curvature of the surface

R_1 = the distance from a source point to the point of reflection, and

θ_1' = the angle between an incident ray and the tangent plane;

then, as shown in Appendix A, if

$$2R_1 - a\sin\theta_i' < 0 \tag{42}$$

the reflected ray diverges and no caustic is formed. This situation is illustrated in Fig. 10(a). Locally the reflected rays appear to be diverging from a virtual source at a distance f from the point of reflection, where

$$f = \frac{R_1 a \sin\theta_i'}{a\sin\theta_i' - 2R_1} \quad . \tag{43}$$

For this case, the far zone reflected field is equal to the reflected field from the tangent plane multiplied by the divergence factor given by

$$D = \sqrt{f/R_1} \quad . \tag{44}$$

On the other hand, if

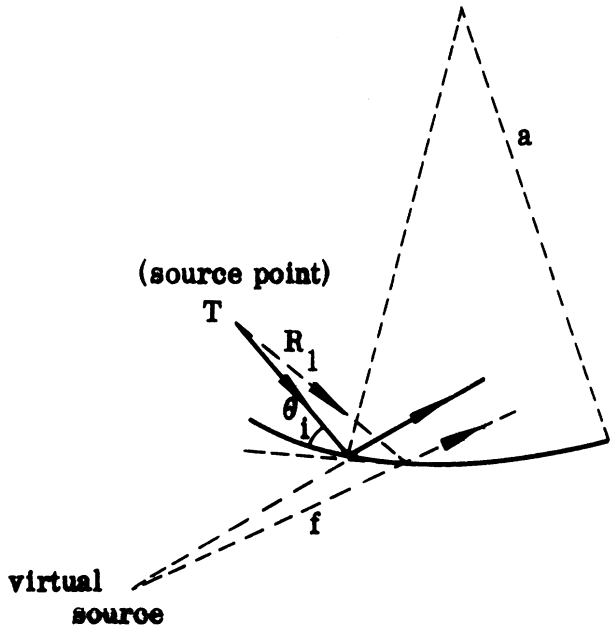

FIG. 10(a): Reflection from a concave surface (no caustic)

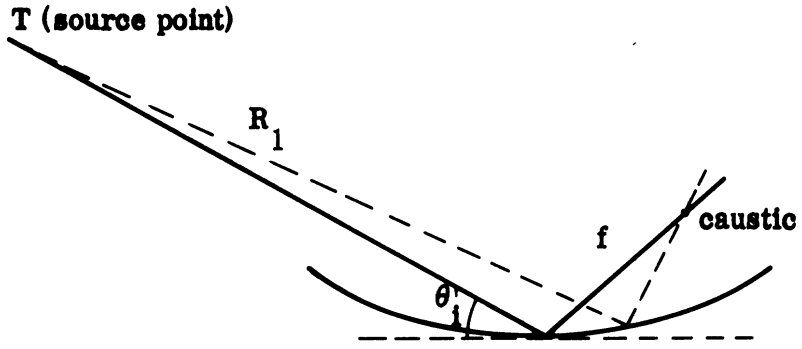

FIG. 10(b): Reflection from a concave surface (caustic formation).

$$2R_1 - a\sin\theta_i' > 0 \quad , \tag{45}$$

the reflected rays form a caustic at a distance

$$f = \frac{R_1 a \sin\theta_i'}{2R_1 - a\sin\theta_i} \tag{46}$$

from the point of reflection. This condition is illustrated in Fig. 10(b). The reflected field strength at the caustic is usually very large, and cannot be predicted by using ray theory. For the present investigation, it is true that we usually have very shallow cavities, so that a is very large and caustics are formed only when θ_i' is very small. Under these conditions, the caustic is usually very low (less than a hundred feet above the ground), so that at higher altitudes the far zone reflected field can again be estimated by using the tangent plane approximation multiplied by the divergence factor $D = \sqrt{f/R_1}$.

Explicitly, if H is the height of the transmitter, then the height of the caustic above the horizon is given by

$$h_c = H - R_1\sin\theta_i + f\sin\theta \tag{47}$$

and the horizontal distance from the transmitter to the caustic is

$$x_c = R_1\cos\theta_i + f\sin\theta \tag{48}$$

where θ is the direction of the reflected ray and $-\theta_i$ is the direction of the incident ray.

Before carrying out an illustrative example on the location of the caustic, it is necessary to investigate (a) the possibility of shadowing, i.e., if a part of the surface is in the shadow region, therefore giving no reflection, and (b) the possibility of multiple reflection, i.e., if some of the reflected rays are obstructed by the concave surface and reflected again before reaching the far zone. Criteria for these possibilities can be deduced geometrically by referring to Fig. 11. As shown in this figure, an incident ray with a depression angle θ_i (angle with horizontal) is

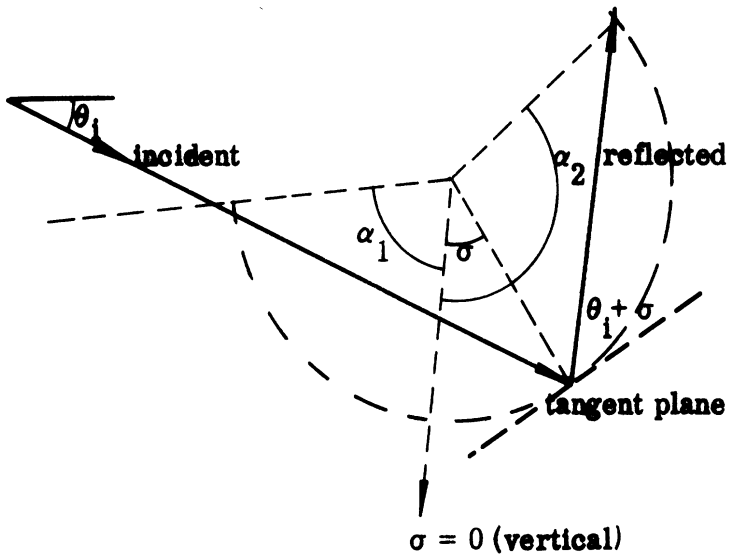

FIG. 11: Diagram to describe the criteria for obtaining various rays.

reflected by a concave cylinder (dotted line) at a point defined by an angle σ measured from a vertical line passing through the axis of the cylinder. It is seen that the incident ray intersects the cylinder at a point defined by the angle

$$-\alpha_1 = -(2\theta_i + \sigma) \tag{49}$$

while the reflected ray intersects the cylinder at a point defined by the angle

$$\alpha_2 = (2\theta_i + 3\sigma) \quad . \tag{50}$$

Thus, for a convex cylinder with angular span

$$\alpha_2 \geq \sigma \geq -\alpha_1$$

the rays with incident direction θ_i such that

$$2\theta_i + \sigma > \alpha_1 \tag{51}$$

are not shadowed, and the rays with θ_i such that

$$2\theta_i + 3\sigma > \alpha_2 \tag{52}$$

are not obstructed.

As an example of estimating the caustic region, let us consider a concave cavity located at a distance D = 2100 ft from an antenna of height H = 35 ft, as sketched in Fig. 12. The cavity is 800 ft wide and 5 ft deep. (The dimensions of this example are taken from the ground profile furnished us by the sponsor.) Assume that the cavity is approximately cylindrical in shape, then the radius a and half angle α_0 of the cylinder may be evaluated from the relations

$$2a \sin\alpha_0 = 5$$

and

$$a(1 - \cos\alpha_0) = 800 \text{ ft} .$$

The solution of the above yields

$$a = 16,002 \text{ ft}$$

and

$$\alpha_0 = 1.432^o .$$

To study the focusing effect of the rays reflected from this cavity, we express the coordinates of every point on the cylinder in parametric form in terms of the angle σ by

$$x = D + a\cos\sigma \tag{53}$$

$$y = a(\cos\alpha_0 - \cos\sigma) \tag{54}$$

with

$$1.432^o = \alpha_0 \geq \sigma \geq -\alpha_0 = -1.432^o .$$

Therefore, the incident direction of a ray reflected at a point σ is given by

$$\theta_i = \tan^{-1} \frac{H - a(\cos\alpha_0 - \cos\sigma)}{D + a\cos\sigma} \tag{55}$$

The corresponding angle of incidence of this ray is

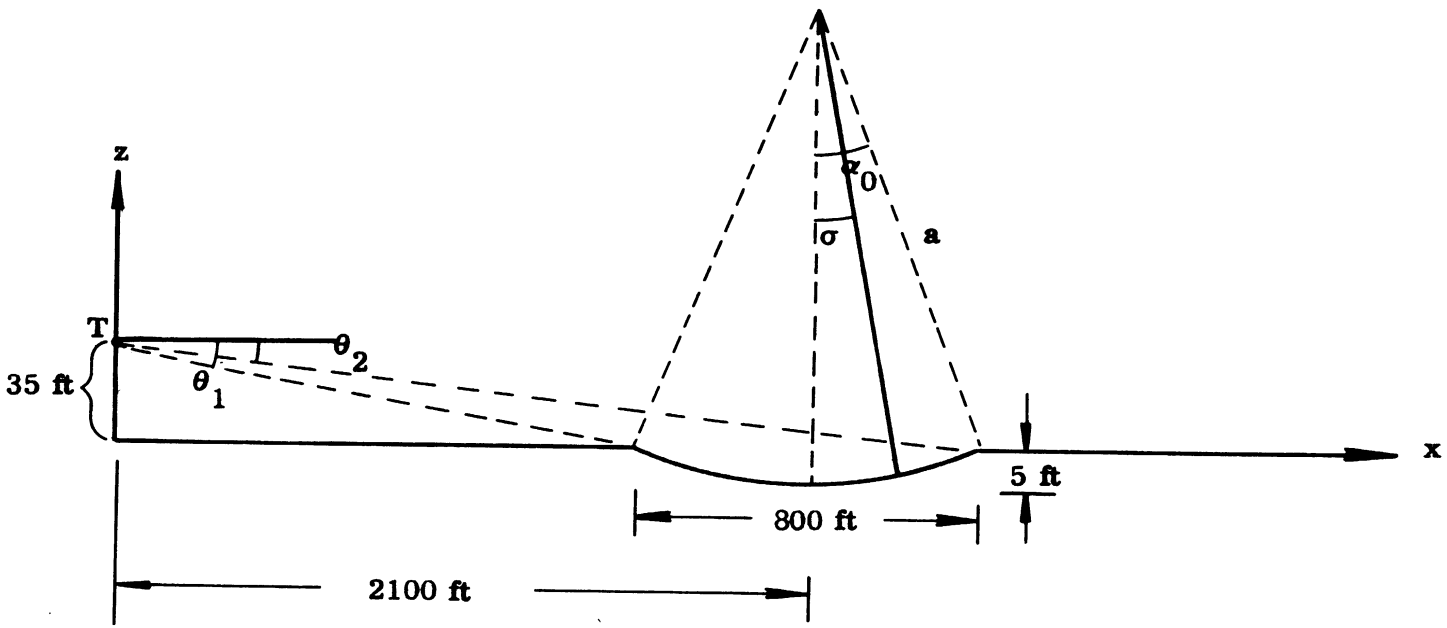

FIG. 12: A concave cavity in the ground profile.

$$\theta_i' = \theta_i + \sigma \tag{56}$$

while the corresponding direction of the reflected ray is

$$\theta = \theta_i + 2\sigma \quad . \tag{57}$$

Moreover,

$$R_1 = \sqrt{\left[H - a(\cos\alpha_0 - \cos\sigma)\right]^2 + (D + a\cos\sigma)^2}$$

and

$$\Delta = 2R_1 \sin^2\theta_i' \quad . \tag{59}$$

From Eqs. (51), (52) and (55), it is found numerically that the points with $1.432^o \geq \sigma \geq -0.274^o$ are illuminated and the rays reflected from these points form a caustic region. Using Eqs. (55) - (58) and (46) - (48), we may construct a table concerning the directions of incident and reflected rays, and the locations of the caustic region. This is given as Table II. From this table, we see that the caustic region is very close to ground, so that for high altitudes, the far zone field Eq. (5) may be used. The example shows that the caustic effects may be neglected for normal flights.

TABLE II

VARIOUS PARAMETERS FOR THE CONCAVE CAVITY PROBLEM

σ (deg)	θ_i (deg)	θ_i' (deg)	θ (deg)	R_1 (ft)	f (ft)	x_c (ft)	h_c (ft)
-0.274	1.127	0.853	0.679	2023.9	126.6	2261.8	-3.32
0	1.091	1.091	1.091	2100.4	164.1	2264.1	-3.50
0.5	1.008	1.518	2.018	2240.0	232.3	2471.8	3.76
1.0	0.904	1.904	2.094	2379.7	299.3	2678.3	12.60
1.432	0.802	2.234	3.666	2501.0	356.4	2855.4	22.80

2.5 Discussion

We have derived the basic theoretical expressions necessary to obtain the effects of various ground profiles on the far field produced by a beacon antenna located above ground. The theory is based on ray optics and neglects any effects of diffraction. Focussing effects of concave cylindrical surfaces are found to be important in regions very close to the horizon. Hence it is believed that such effects will not be of significance for normal ATCRBS operation.

Based on the formulation developed here, a general computer program can be developed to obtain the far field lobing patterns and other pertinent results for given antenna and ground profiles. The ground profile will be synthesized by sections of planar surfaces with linear slopes and cylindrical surfaces. This is discussed in the next section.

3. THE EFFECTS OF GROUND PROFILE ON ATCRBS PERFORMANCE: DEVELOPMENT OF THE COMPUTER PROGRAM

3.1 Introduction

General theoretical formulation and the derivation of various expressions necessary to obtain the effects of ground profile in the far field patterns of ATCRBS antennas located above ground have been discussed in Section 2. In the present section we develop a computer program, based on the formulation discussed in Section 2, calculate the various quantities characterizing the performance of an ATCRBS in the presence of a ground whose profile may be approximated by sections of planar surfaces. It is assumed that the free space pattern of the ATCRBS antenna is known. For the present, we neglect the effects of diffraction, multiple reflection and the curvature of the ground. Only the SLS mode performance of ATCRBS is considered here. The quantities of interest are: P1 and P2 pulse patterns, P1/P2 pulse ratio patterns, effective azimuth beamwidth, the number of replies and the coverage diagram. The computer program is developed such that the output data and format correspond to the general ATCRBS computer program discussed in our earlier reports [1, 2].

3.2 Basic Expressions

Let the ground profile in the x-z plane, where x is the horizontal axis, be as shown in Fig. 13. The points on the ground where the ground profile changes its slope and/or its refractive index are denoted by the set of points (x_j, z_j), $j = 1, 2, 3, \ldots, M$. Each ground section is assumed to be planar with a given slope between (x_j, z_j) and (x_{j+1}, z_{j+1}) and level (slope = 0) beyond the point (x_M, z_M) as shown in Fig. 13. Note that the ground profile is assumed to be independent of the y-coordinate. Thus, the ground is approximated by (M+1) sections of planar surfaces. The first section is between (0, 0) and (x_1, z_1) having a slope given by

$$\alpha_1 = \tan^{-1}(z_1/x_1) \ , \tag{60}$$

and the slope of the jth section, located between (x_{j-1}, z_{j-1}) and (x_j, z_j), is

MISSING
PAGE

$$\alpha_j = \tan^{-1}\left(\frac{z_j - z_{j-1}}{x_j - x_{j-1}}\right) , \qquad j = 1, 2, \ldots, M . \tag{61}$$

The (M+1)th section located beyond the point (x_M, z_M) is assumed to be horizontal and consequently

$$\alpha_{M+1} = 0 . \tag{62}$$

The set of equations (60) - (62) completely specifies a given ground profile approximated by linear sections.

The index of refraction for each section of ground is assumed to be known and is given by N_j such that

$$N_j = \sqrt{\epsilon_j} , \tag{63}$$

where ϵ_j is the relative permittivity of the jth ground section.

It is assumed that the antenna under study is located on the z-axis and at a height H above the horizontal axis, as shown in Fig. 13. The field at any far zone point located at an elevation angle θ will be the sum of the contributions due to a direct ray from the antenna in the direction θ and a ray (or rays) from the antenna and reflected by a ground section (or sections) in the direction θ. The direct ray and a ray reflected by the jth ground section in the direction of the far field point are shown in Fig. 14. Let an incident ray with depression angle θI_j, after reflection by the jth ground section, has an elevation angle θ so that it reaches the far field point. For any given angle θ, the corresponding depression angle of the incident ray may be obtained from Fig. 14 and is given by

$$\theta I_j = \theta - 2\alpha_j , \tag{64}$$

where α_j is the slope of the jth ground section defined before. To obtain the reflection coefficient of a ground section let us denote the angle of incidence at the jth section by θP_j as shown in Fig. 14. It can be shown that

MISSING
PAGE

$$\theta P_j = \theta - \alpha_j \quad . \tag{65}$$

For vertically polarized incident waves, the Fresnel coefficient of reflection is given by [3]:

$$\rho_j = \frac{N_j^2 \sin(\theta P_j) - \sqrt{N_j^2 - 1 + \sin^2(\theta P_j)}}{N_j^2 \sin(\theta P_j) + \sqrt{N_j^2 - 1 + \sin^2(\theta P_j)}} \quad . \tag{66}$$

Note that, in general, ρ_j is complex and Eq. (66) is valid for both real and complex values of N_j.

To calculate the phase of the reflected field relative to the direct field caused by the propagation path difference, let us denote by HP_j the distance between the antenna and the point of intersection on the z-axis of the extended jth section profile, as shown in Fig. 14. It can be shown that HP_j may be obtained from

$$HP_j = H - z_{j-1} + x_{j-1} \tan\alpha_j \quad . \tag{67}$$

The path difference between the direct ray and the ray reflected in the θ-direction by the jth section of the ground may be expressed in terms of HP_j and is given by:

$$\Delta_j = 2HP_j \cos(\alpha_j) \sin(\theta P_j) \quad . \tag{68}$$

The electric field at a far field point (R, θ) due to the ray reflected by the jth section of the ground may now be written in the following form:

$$E_{r_j} = A \frac{e^{i\beta R}}{R} K_j f_d(-\theta I_j) \quad , \tag{69}$$

where

$i = \sqrt{-1}$,

A is a constant,

$\beta = 2\pi/\lambda$ is the free space propagation constant,

$f_d(\theta)$ is the free space elevation plane pattern of the antenna,

$$K_j = \rho_j e^{-i\beta\Delta_j} , \tag{70}$$

ρ_j is the reflection coefficient as defined by Eq.(66).

The total field at (R, θ) consists of the direct field and the field reflected in the θ-direction by the ground sections and can now be written as

$$E(R,\theta)_{Total} = A\left[f_d(\theta) + \sum_{j=1}^{M+1} K_j f_d(-\theta I_j)\right]\frac{e^{i\beta R}}{R} . \tag{71}$$

Given any θ and a ground profile it is possible to calculate the incident angle θI_j (or θP_j) such that the ray reflected from the jth section, if the section extends from $x = 0$ to $x = \infty$, is in the direction θ. Of course, in actual cases not all θI_j are physically possible due to the following: (a) the finite extent of each ground section and (b) the possibility of geometrical shadowing. To obtain the criteria for the occurrence of the nonphysical values of θI_j let us refer to Fig. 15 and define the depression angle corresponding to (x_j, z_j) by

$$s_j = \tan^{-1}\frac{H - z_j}{x_j} . \tag{72}$$

It is evident from Fig. 15 that if

$$\theta I_j < s_j \qquad \text{or} \qquad \theta I_j > s_{j-1} \tag{73}$$

then there is no reflection from the jth section due to its finite size or, in other words, acceptable incident angles θI_j for the jth section must lie in the range $s_{j-1} < \theta I_j < s_j$.

As shown in Fig. 16, if for any $k < j$,

$$\theta I_j > s_k \tag{74}$$

the incident ray is shadowed and there will be no reflection.

MISSING PAGE

MISSING PAGE

Combining Eqs. (73) and (74) we find that if

$$\theta I_j < s_j \qquad \text{or} \qquad \theta I_j > s_k, \quad k < j \tag{75}$$

then

$$K_j \equiv 0 \quad . \tag{76}$$

Equations (75) and (76) indicate that for the incident ray whose depression angle satisfies Eq. (75) cannot reach the far field point by single reflection from the jth ground section.

Even if Eq. (75) is not satisfied, there may exist cases such that the reflected ray is obstructed by the ground and does not reach the far zone field point. Such a situation of "ray obstruction" is depicted in Fig. 17, which shows a ray reflected from the jth section obstructed by the kth section ($k > j$). This can occur if $D_j > T_k$ where the intercepts D_j and T_k on the z-axis are as defined in Fig. 17. For a given angle θ and the ground profile, these intercepts may be obtained from the following relations:

$$T_k = x_k \tan\theta - z_k \tag{77}$$

$$D_j = \frac{HP_j\left[\tan(\theta I_j)+\tan\theta\right]}{\left[\tan(\theta I_j)+\tan\alpha_j\right]} - H. \tag{78}$$

The condition for the obstruction of the reflected ray can therefore be stated as follows:

$$\begin{aligned} &\text{if } D_j > T_k, \qquad k > j \\ &\text{then} \qquad K_j \equiv 0 \end{aligned} \tag{79}$$

When Eq. (79) is satisfied, a reflected ray may reach the far field point only after multiple reflection. Such cases are neglected in the present investigation.

MISSING PAGE

3.3 Various Quantities of Interest

In the previous section we have discussed the method of obtaining the field at a far zone point produced by an ATCRBS antenna in the presence of a ground of given profile. From the knowledge of this field, various quantities of interest characterizing the performance of an ATCRBS may be obtained. In the present section we give the appropriate expressions for the desired quantities. Detailed discussions of the derivations of these expressions have been given in [1, 2] and will not be repeated here.

The intensities of the P1 and P2 pulses at the far field point (R, θ) are defined to be the magnitudes of the total electric fields produced by the directional and omnidirectional antennas, respectively, and located at appropriate heights above ground.

After using Eq. (71) and assuming $A = 1$, the following is obtained for the SLS mode P1 pulse amplitude as a function of the elevation angle:

$$P1(\theta)_{SLS} = \left| f_d(\theta) + \sum_{j=1}^{M+1} K_j f_d(-\theta I_j) \right| = F_d(\theta) \quad \text{(say)} \tag{80}$$

where the various notations used are as defined before. In the SLS mode only, the directional antenna radiates the P1 pulse and hence, $f_d(\theta)$ in Eq. (21) represents the elevation plane free space pattern of the directional antenna of ATCRBS.

Assuming that the nominal pulse ratio is K_0 (U.S. standards require that $K_0 = 18\text{dB}$), it can be shown that the P2 pulse pattern produced by the omnidirectional antenna is given by

$$P2(\theta) = \frac{1}{K_0} \left| f_0(\theta) + \sum_{j=1}^{M+1} K_j f_0(-\theta I_j) \right| = F_0(\theta)/K_0 \quad \text{(say)} \tag{81}$$

where $f_0(\theta)$ is the elevation plane free space pattern of the omnidirectional antenna. In obtaining K_j and θI_j in Eq. (81) from the expressions given in the previous sections it should be noted that the antenna height parameter H should correspond to that of the omnidirectional antenna.

From Eqs. (80) and (81) the pulse ratio at the far field point is given by

$$\frac{P1(\theta)}{P2(\theta)} = K_0 \frac{F_d(\theta)}{F_0(\theta)} \quad . \tag{82}$$

Instead of representing the absolute value of the pulse ratio given by Eq. (82), it is found more convenient to use the normalized pulse ratio concept and express it in dB, as follows:

$$\begin{aligned} \text{normalized } P1/P2 &= 20 \log_{10} \frac{P1(\theta)}{P2(\theta)} - 20 \log_{10} K_0 \\ &= 20 \log_{10} \frac{F_d(\theta)}{F_0(\theta)} \quad . \end{aligned} \tag{83}$$

The effective azimuth beamwidth ϕ_{eff} of ATCRBS is an important concept and was discussed in [1, 2]. Targets within ϕ_{eff} will reply and those outside will not. Assuming that the main beam killing thresshold level is a, it can be shown that for a directional antenna having a Gaussian gype of azimuthal pattern, the effective azimuth beamwidth is given by

$$\phi_{eff} = 2\phi_0 \left[\frac{20 \log_{10} \frac{P1(\theta)}{P2(\theta)} - a(dB)}{12.0735} \right]^{1/2} \tag{84}$$

where ϕ_0 is the total half-power beamwidth of the azimuthal pattern of the directional antenna.

The number of replies from the transponder is now defined as

$$N = f_i \frac{\phi_{eff}}{\Omega} \quad , \tag{85}$$

where f_i is the interrogator pulse repetition,

Ω is the angular scanning rate in deg/sec.

Typical values of f_i and Ω are: f_i = 360 pulses/sec, $\Omega = 90^o$/sec for terminal installation and 36^o/sec for enroute installation.

If it is assumed that the free space range R_0 of ATCRBS is given as a known parameter of the system, then it can be shown that the range as a function of the elevation angle θ, i.e., the coverage diagram, is given by

$$R(\theta) = R_0 F_d(\theta)$$

$$= R_0 \left| f_d(\theta) + \sum_{j=1}^{M+1} K_j f_d(-\theta I_j) \right|^{1/2} . \qquad (86)$$

3.4 Computation Scheme

Based on the discussions given in section 3.2 and 3.3 we develop the following scheme for computing the various quantities characterizing the performance of ATCRBS.

3.4.1 Given Parameters

For the present we shall consider only two antenna systems: the Hazeltine open array and the existing (or Hog-Trough) antennas. For both the antennas the free space elevation plane patterns of the directional and omnidirectional antennas match, i.e., $f_d(\theta) = f_0(\theta)$. However, the phase center of the omhidirectional antenna of each system lies above that of the directional antenna. The pattern characteristics of these antennas are discussed in [1]. Here we quote only the relevant expressions and results necessary for the present computation.

The elevation plane pattern of the Hazeltine open array antenna is obtained from the following expression:

$$f_d(\theta) = \sum_{n=0}^{3} f_{d_1}(\theta_n) \frac{\sin \pi \left[\frac{\sin(\theta - \theta_0)}{0.225} - n \right]}{\pi \left[\frac{\sin(\theta - \theta_0)}{0.225} - n \right]} , \qquad (87)$$

where θ_0 is the tilt angle of the antenna beam (normally $\theta_0 = 0$) and θ_n and $f_{d_1}(\theta_n)$ are given in Table III.

TABLE III
SAMPLED VALUES OF THE PATTERN FUNCTION
FOR THE HAZELTINE OPEN ARRAY ANTENNA

n	θ_n^o	$f_{d_1}(\theta_n)$
0	0	0.500
1	13	1.000
2	26.75	0.855
3	42.4	0.530

The analytical expression to compute the free space elevation plane pattern of the existing antenna is given by:

$$f_d(\theta) = \sum_{n=-2}^{n=+2} f_{d_1}(\theta_n) \frac{\sin \pi \left[\frac{\sin(\theta - \theta_0)}{0.47767} - n \right]}{\pi \left[\frac{\sin(\theta - \theta_0)}{0.47767} - n \right]} , \tag{88}$$

where θ_n and $f_{d_1}(\theta_n)$ are shown in Table IV.

TABLE IV
SAMPLED VALUES OF THE PATTERN FUNCTION
FOR THE EXISTING ANTENNA

n	θ_n^o	$f_{d_1}(\theta_n)$
-2	-72.8	0.084
-1	-28.55	0.510
0	0	0.966
1	28.55	0.780
2	72.8	0.045

The other pertinent characteristics of the two antennas that may be of later use are given in Table V. In addition, the free space propagation constant β, the refractive index N_j $(=\sqrt{\epsilon})$ and the ground profile (x_j, z_j), $j = 1, 2, \ldots, M$ are also known parameters in a given situation.

TABLE V

SOME CHARACTERISTICS OF THE HAZELTINE OPEN ARRAY AND EXISTING ANTENNAS AT 1030 MHz

	Hazeltine	Existing
Height of the directional antenna	33 feet	31.5 feet
Height of the omnidirectional antenna	37 feet	33.0 feet
Gain (over isotropic)	23 dB	21 dB
Horizontal beamwidth	2.45^{o}	2.35^{o}
Vertical beamwidth	29^{o}	50^{o}
Field gradient (elevation pattern roll-off) at -6 dB	1.14 dB/deg	0.37 dB/deg.
Azimuth plane sidelobes	-25 dB	-25 dB

3.4.2 Computation

Once the input parameters are known the computation of the various quantities can proceed as follows.

(i) Slopes

$$\alpha_1 = \tan^{-1} z_1/x_1 \tag{60}$$

$$\alpha_j = \tan^{-1} \frac{z_j - z_{j-1}}{x_j - x_{j-1}} \quad , \qquad j = 1, 2, \ldots, M \tag{61}$$

$$\alpha_{M+1} = 0$$

(ii) Depression angles

$$s_j = \tan^{-1} \frac{H - z_j}{x_j} \tag{72}$$

$$s_{M+1} = 0 \tag{72'}$$

(iii) Intercepts

$$HP_j = H - z_{j-1} + x_{j-1} \tan\alpha_j \tag{67}$$

(iv) Direct field pattern

Choose an incremental angle $\Delta\theta$, and let $\theta = n\Delta\theta$, $n = 0, 1, 2, 3, \ldots$. For each θ compute $f_d(\theta)$ appropriate for the given antenna, i.e., use Eqs. (87) and (88).

(v) Incident ray directions

For a given θ, calculate

$$\theta I_j = \theta - 2\alpha_j \tag{64}$$

and

$$\theta P_j = \theta - \alpha_j \ . \tag{65}$$

(vi) Test for "condition of no reflection"

If

$$\theta I_j < s_j \quad , \quad \text{or}$$
$$\theta I_j > s_{j-1} \ , \quad s_{j-2}, \ldots, s_1 \tag{75}$$

set

$$K_j = 0 \tag{76}$$

(vii) Test for "condition of obstruction"

For the remaining set of θI_j and j, compute

$$D_j = \frac{HP_j\left[\tan(\theta I_j) + \tan\theta\right]}{\left[\tan(\theta I_j) + \tan\alpha_j\right]} - H \tag{78}$$

and

$$T_j = x_j \tan\theta - z_j \ . \tag{77}$$

If

$$T_j > D_{j+1} \ , \quad D_{j+2}, \ldots, D_m \tag{79}$$

set

$$K_j = 0 \ .$$

(viii) Reflected field

For the remaining set of θi_j and j, compute

$$\rho_j = \frac{N_j^2 \sin(\theta P_j) - \sqrt{N_j^2 - 1 + \sin^2(\theta P_j)}}{N_j^2 \sin(\theta P_j) + \sqrt{N_j^2 - 1 + \sin^2(\theta P_j)}} \quad , \tag{66}$$

$$\Delta_j = 2HP_j \cos(\alpha_j) \sin(\theta P_j) \tag{68}$$

$$K_j = \rho_j e^{-i\beta\Delta_j} \tag{70}$$

and $$f_d(-\theta I_j) \tag{87 or 88}$$

(ix) Various patterns

$$P1(\theta) = \left| f_d(\theta) + \sum_{j=1}^{M+1} K_j f_d(-\theta I_j) \right| = F_d(\theta) \tag{80}$$

$$P1(\theta) \text{ in dB} = 20 \log_{10} F_d(\theta)$$

$$P2(\theta) = \frac{1}{K_0} \left| f_0(\theta) + \sum_{j=1}^{M+1} K_j F_0(-\theta I_j) \right| = F_0(\theta)/K_0 \tag{81}$$

$$P2(\theta) \text{ in dB} = 20 \log_{10} F_0(\theta) - K_0$$

$$\text{normalized } P1/P2 = 20 \log_{10} \frac{F_d(\theta)}{F_0(\theta)} \tag{83}$$

$$\phi_{eff} = 2\phi_0 \left[\frac{20 \log_{10} \frac{P1(\theta)}{P2(\theta)} - a\ (dB)}{12.0735} \right]^{1/2} , \qquad (a = 9) \qquad (84)$$

$$N = f_i \frac{\phi_{eff}}{\Omega} \quad . \qquad (85)$$

The computer output is digital as well as graphical. The computer program along with the flow chart and the various symbols used are given in Appendix B.

4. NUMERICAL RESULTS AND DISCUSSION

4.1 Introduction

The computer program developed in the previous section is used to obtain some results to illustrate the effects of some given ground profiles on the SLS mode performance of ATCRBS using the Hazeltine open array antenna. Pertinent pattern characteristics of the interrogator antenna system are as discussed in Section 3.4 The ground is assumed to have a dielectric constant $\epsilon_r = 3.0$. Section 4.2 considers a simple ground profile consisting of two planar sections. The results for this ground profile illustrate the power and the capabilities of the computer program and they also identify some of the effects of simple terrain features on the ATCRBS performance. Section 4.3 considers a more complicated ground profile consisting of a number of planar sections; the profile is prepared such that it approximates some typical terrain profile as seen by an aircraft during a radial flight over the NAFEC area. The computed results are compared with those obtained by actual flight tests.

4.2 Illustrative Examples

In this section we consider the ATCRBS to be located above a ground consisting of two planar sections, as shown in Fig. 18, each having the same dielectric constant $\epsilon_r = 3.0$. As discussed earlier the far zone fields (the P1 and P2 pulses in the far zone are proportional to these fields) consist of the direct fields from the antenna and the fields reflected from the two sections of the ground. In terms of the reflected components of fields it is found convenient to divide the elevation plane of interest into the following three zones.

Zone B: $0 \leq \theta \leq \theta_c - 2\alpha_1$. In this zone, the far field consists of the direct field and a field reflected from the ground section B only.

Zone BC or Transition Zone: $\theta_c - 2\alpha_1 < \theta < \theta_c + 2\alpha_1$. In this zone the far field consists of the direct field and fields reflected from both the ground plane sections B and A.

Zone A: $\theta_c + 2\alpha_1 \leq \theta \leq \pi/2$. In this zone the far field consists of the direct field and a field reflected from the ground section A only.

MISSING PAGE

In the above definitions, the angles θ_c and α_1 are as shown in Fig. 18 and are given by

$$\theta_c = \tan^{-1} \frac{H - z_1}{x_1} \tag{89}$$

$$\alpha_1 = \tan^{-1}(z_1/x_1) \quad . \tag{90}$$

Figure 19 shows the P1 and P2 pulse patterns for a ground profile having $\alpha_1 \simeq -0.5^o$, i.e., $x_1 = 600'$, $z_1 = -5.0'$. The corresponding pulse patterns when the antenna is located above a flat ground aligned along the x-axis and also the free space pulse patterns are shown in Fig. 19 for ready comparison.

Discontinuities in the pulse patterns (points marked C, C) for the discontinuous ground case occur approximately within the transition zones corresponding to the height of the P1 and P2 pulse radiating antennas. From this definition, the location and extent of the transition zone varies with the height of the antenna. In the present case for θ lying within the transition zone, two reflected rays contribute to the far field. As a result of this the maxima and minima are more pronounced within this region. This is evident in Fig. 19. For the ground profile and the antenna heights considered, the transition zones occur in $2^o38' \leq \theta \leq 4^o38'$ and $3^o \leq \theta \leq 5^o$ for the P1 and P2 pulses, respectively. The results shown in Fig. 19 are in agreement with the above zones. Outside the transition zone, the P1 and P2 pulse patterns for the discontinuous ground are not changed much in amplitude but the locations of the maxima and minima are shifted relative to the patterns for the flat ground condition. Figure 20 shows the P1 and P2 pulse patterns in the range $0 \leq \theta \leq 20^o$ for the discontinuous ground; larger amplitude maxima and deeper minima in the patterns within the transition zones should be noticed. For $\theta \geq 8^o$ the pulse patterns assume their corresponding free space values.

Figure 21 shows the normalized pulse ratio patterns for the flat and discontinuous ground. Outside the transition zone region, the two pulse ratio patterns are not changed appreciably in amplitude but they are shifted from each other slightly. Within the transition zone, the P1/P2 pattern for the discontinuous ground

MISSING
PAGE

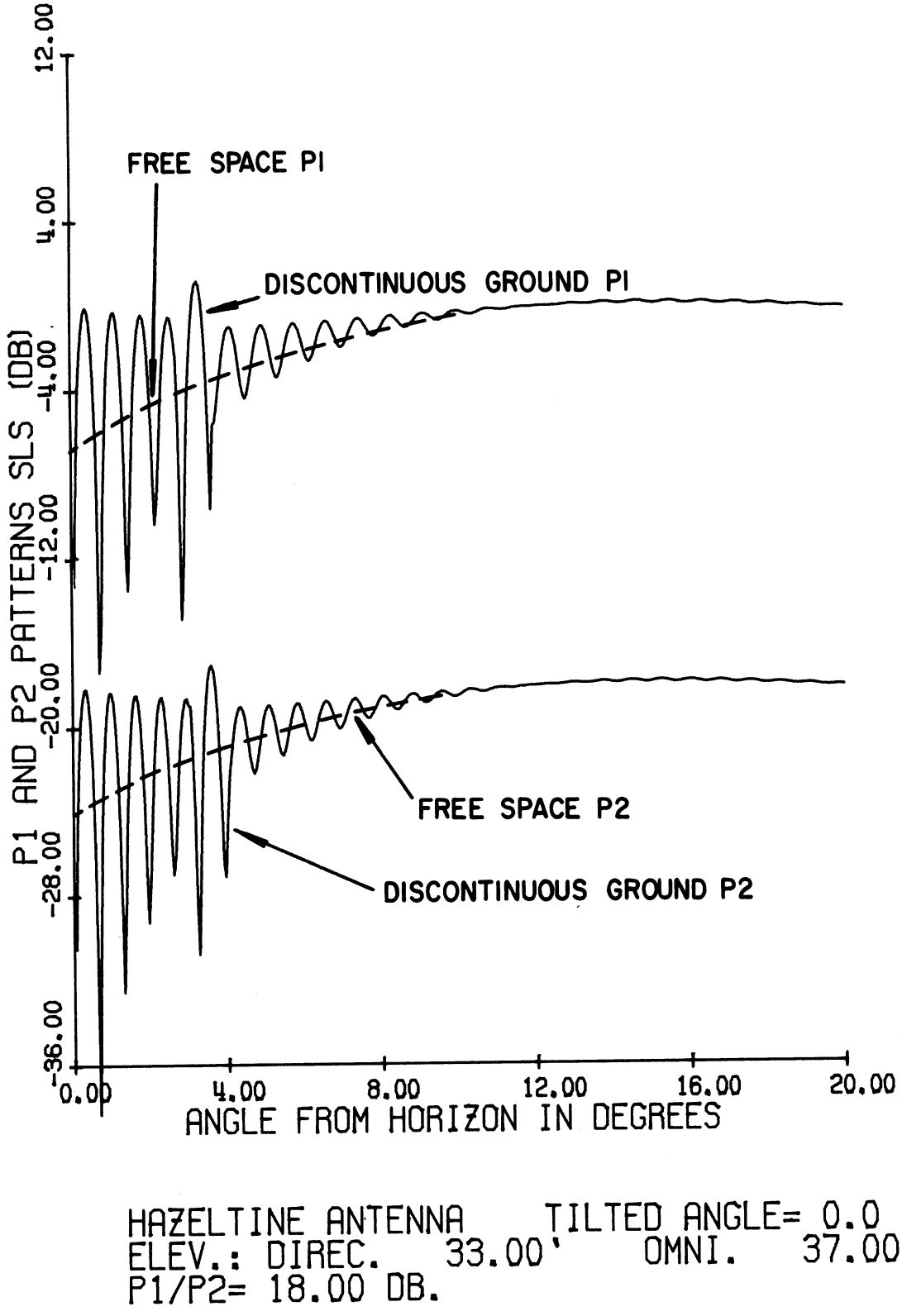

FIG. 20: P1 and P2 pulse patterns above a discontinuous ground. Slope of section A is $\alpha_1 \simeq -0.5^{o}$ ($x_1 = 600'$, $z_1 = -5.0'$).

MISSING PAGE

shows a large amount of oscillation. This implies that both mainbeam killing and sidelobe punch-through will be quite severe within this range of space. Figure 22 shows the pulse ratio pattern in the range $0 \leq \theta \leq 20^{o}$ for the discontinuous ground.

Figures 23 and 24 show the pulse and pulse ratio patterns for the flat and discontinuous ground, respectively, with section A having a slope of -1.0^{o}. Similar results are shown in Figs. 25 and 26 when the section A has a slope of -1.5^{o}. The increased slope seems to increase the shift in the patterns outside the transition zone, particularly for small θ and within the transition region the oscillations are not as strong as those for small slope angles. Similar comment applies to the pulse ratio patterns.

In order to bring out the effects of the extent of the section A we keep the slope of section A constant and increase the values of x_1, z_1. For example, Fig. 27 shows the pulse patterns for a discontinuous ground with $x_1 = 800'$ and $z_1 = -6.7'$ (slope -0.5^{o}). The general behavior of the results is similar to that shown in Fig. 19; however, due to increased values of x_1, z_1, the transition zones have moved towards similar values of θ. For the parameters used, $\theta_c \sim 2^{o}50'$ and $3^{o}8'$ for P1 and P2 pulse patterns, respectively, and the corresponding transition zones are $1^{o}50' \leq \theta \leq 4^{o}8'$. The pulse ratio patterns for the flat and discontinuous ground are shown in Fig. 28. In this case it is found that within the transition zone the pulse ratio shows very strong amplitude oscillations.

4.3 Performance of ATCRBS at NAFEC

In this section we discuss the performance of an ATCRBS using the Hazeltine open array antenna system and located at National Aviation Facilities Experimental Center (NAFEC) of New Jersey. Figure 29 shows a typical terrain profile as seen by an aircraft during a flight at constant height and along a 305^{o} radial from the ATCRBS. This profile has been supplied to us by FAA. The profile is shown in terms of height in feet above sea level versus the distance in feet from the origin, which is located 60 feet above sea level as shown in Fig. 29.

Theoretical P1 and P2 pulse amplitude patterns are shown in Fig. 30. Corresponding patterns for the free space and x-axis oriented flat earth cases are shown in Fig. 30 for comparison. The normalized pulse ratio patterns for the NAFEC

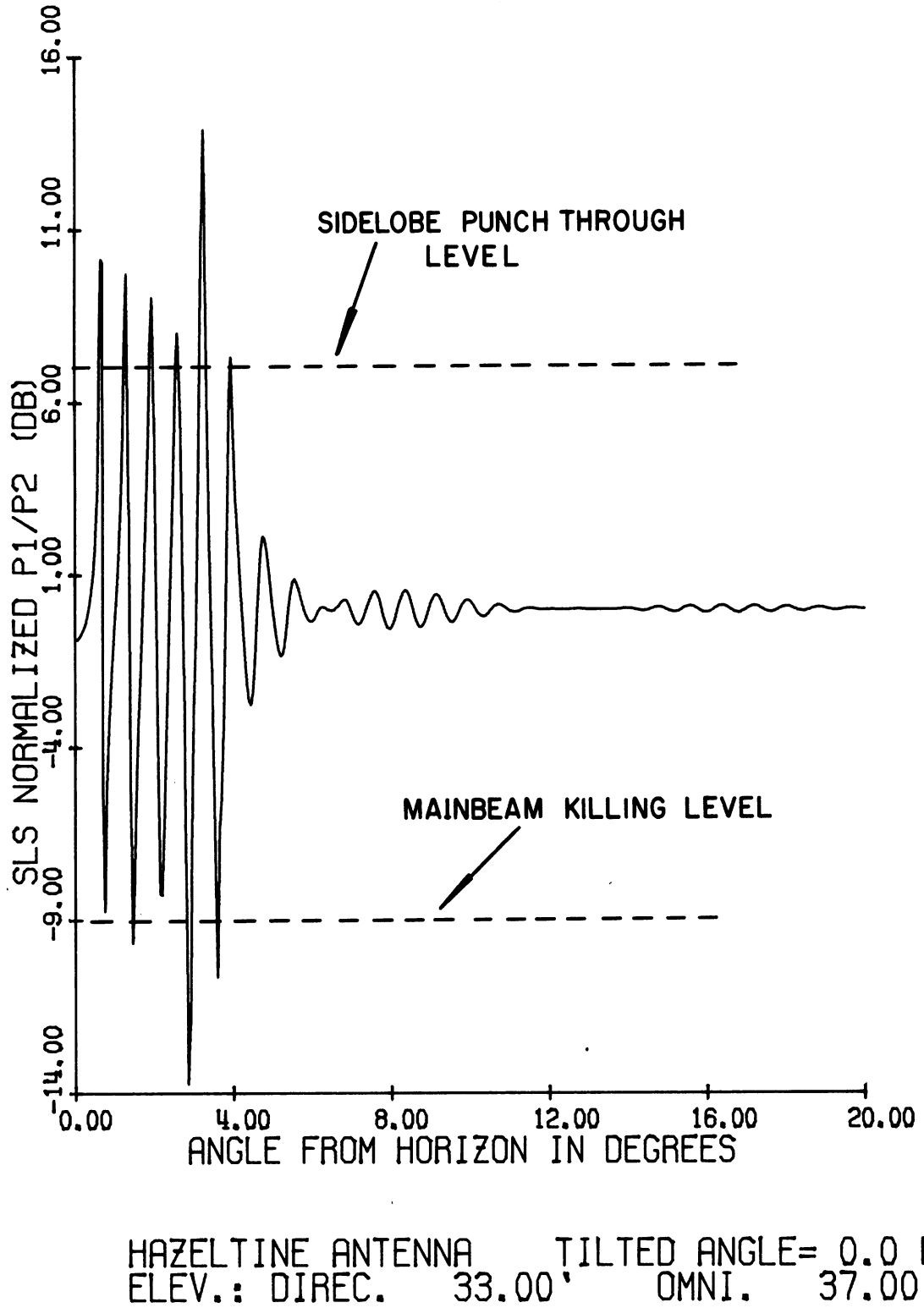

FIG. 22: P1/P2 pattern above a discontinuous ground. Slope of section A is $\alpha_1 \simeq -0.5^{o}$ ($x_1 = 600'$, $z_1 = -5.0'$).

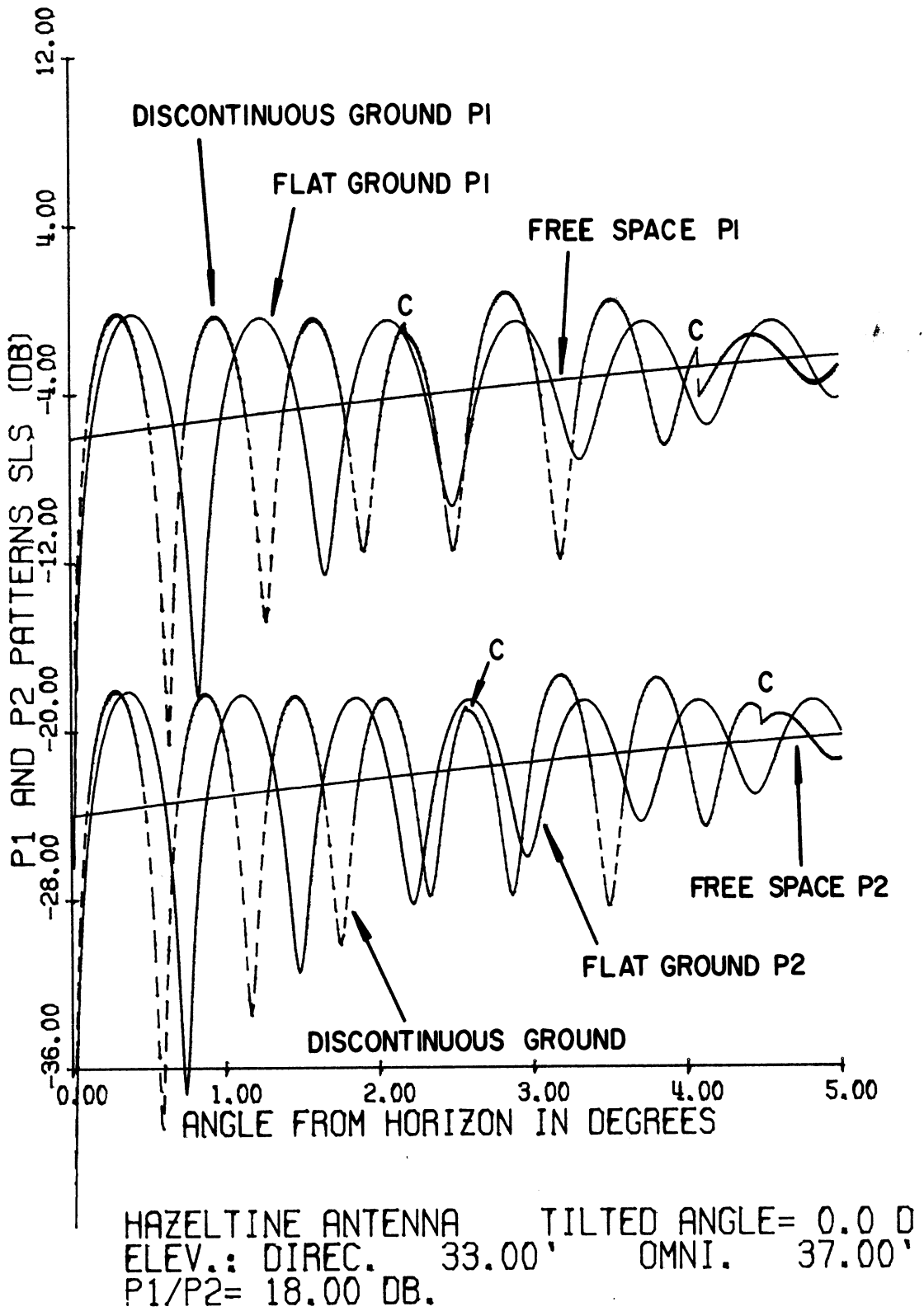

FIG. 23: P1 and P2 pulse patterns in free space and above flat and discontinuous ground. Slope of section A is $\alpha_1 \simeq -1.0^o$ ($x_1 = 600'$, $z_1 = -10'$).

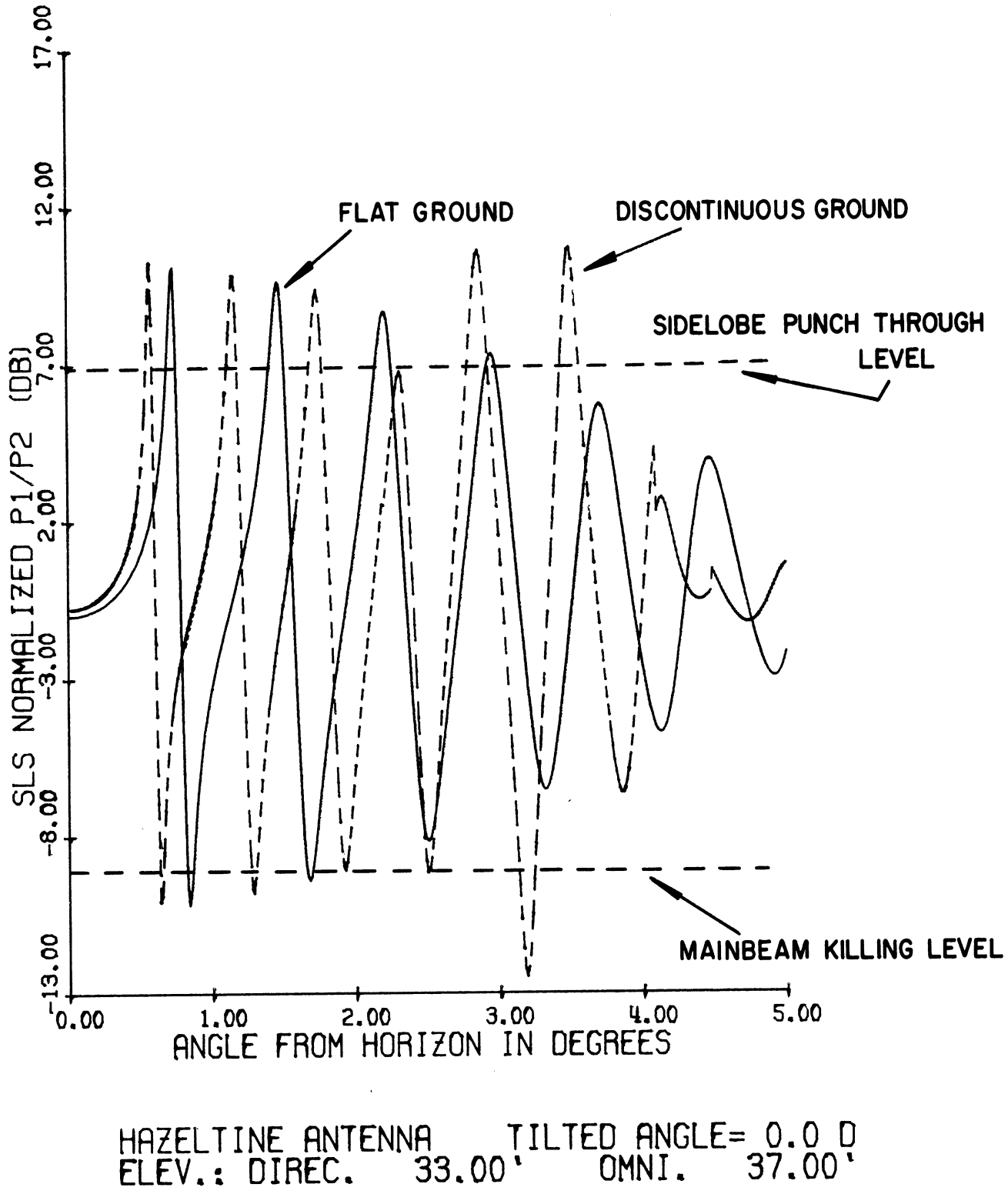

FIG. 24: P1/P2 patterns above flat and discontinuous ground. Slope of section A is $\alpha_1 \simeq -1.0^{o}$ ($x_1 = 600'$, $z_1 = -10'$).

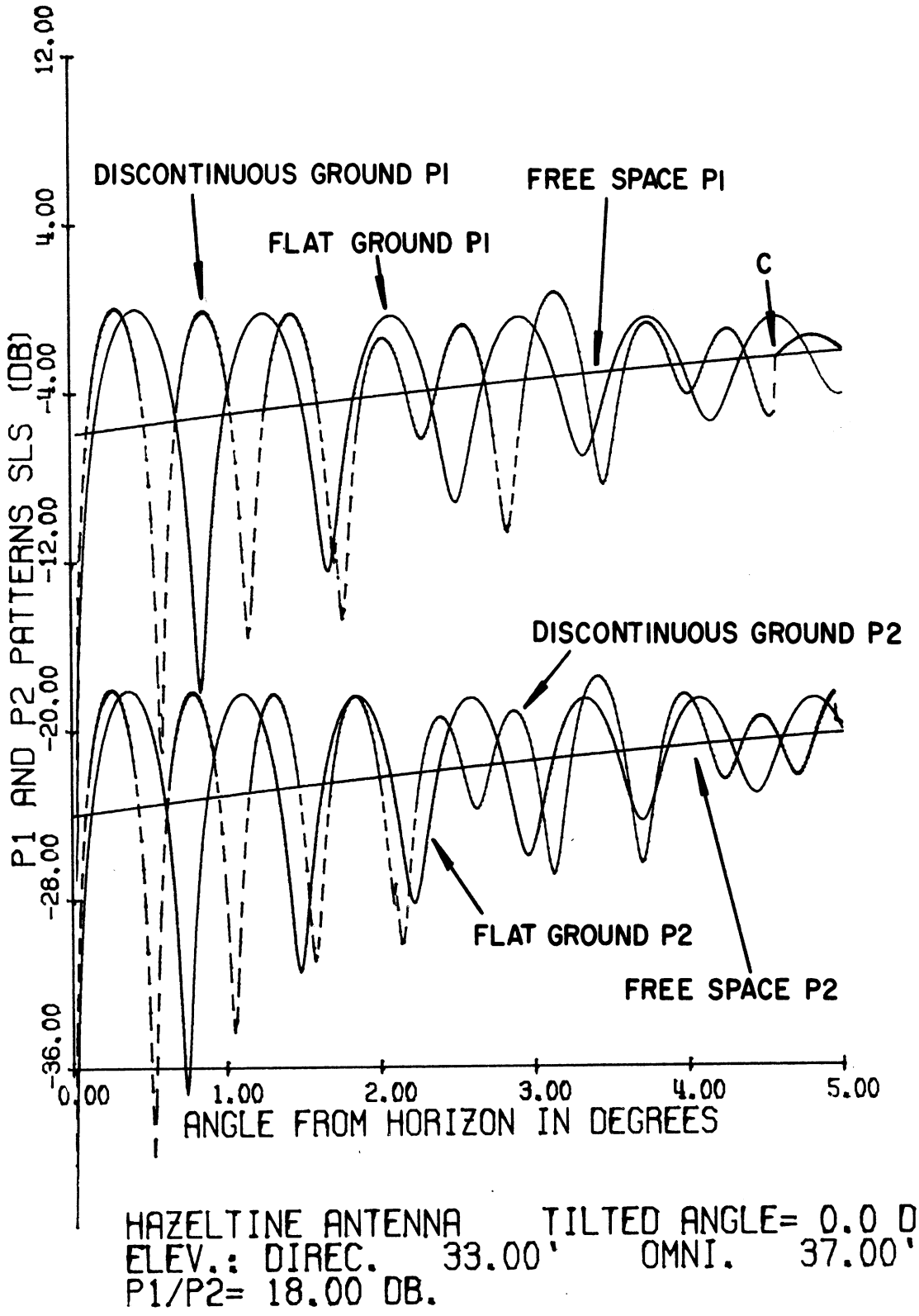

FIG. 25: P1 and P2 pulse patterns in free space and above flat and discontinuous ground. Slope of section A is $\alpha_1 \simeq -1.5^{o}$ ($x_1 = 600'$, $z_1 = -15'$).

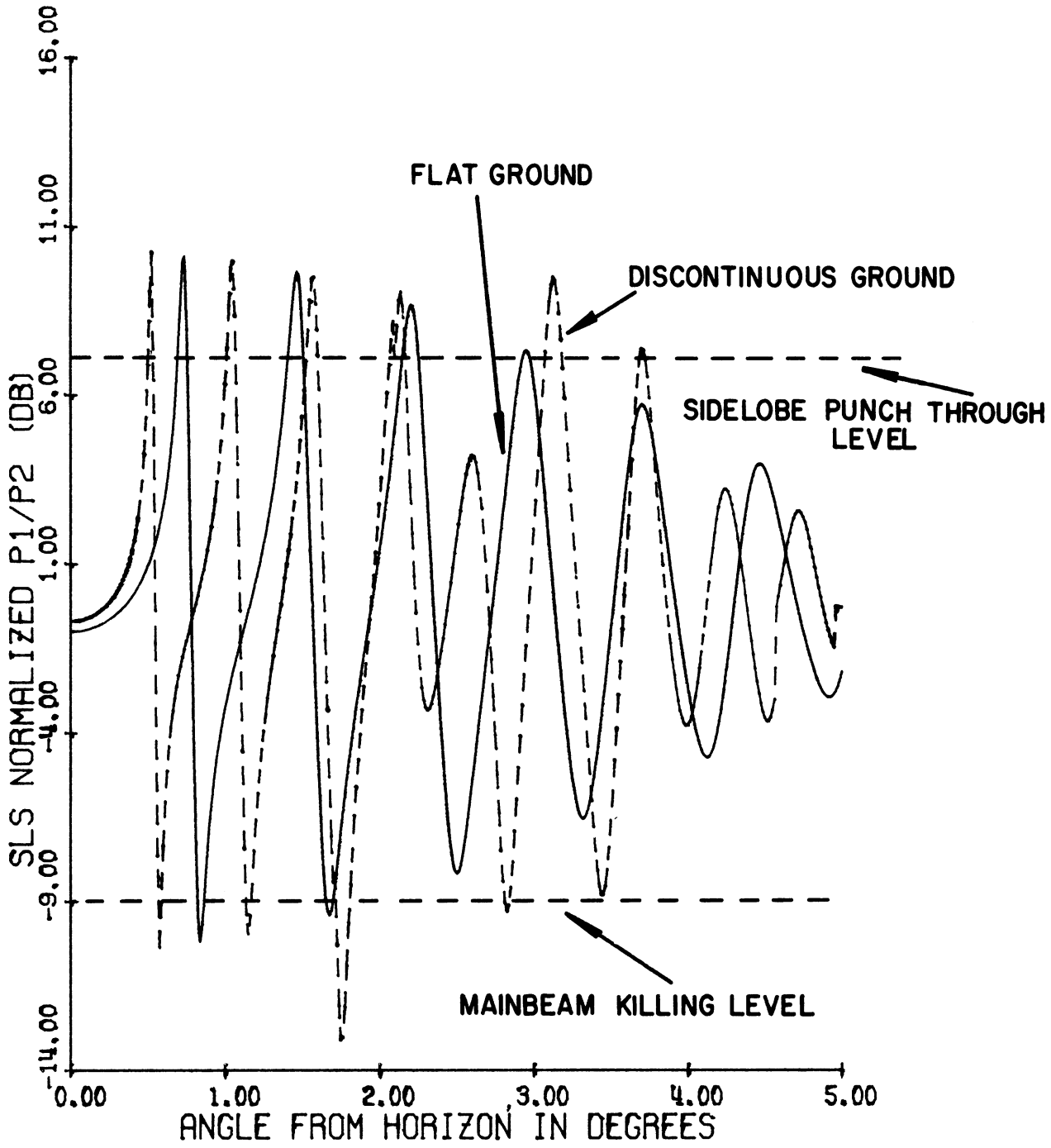

FIG. 26: P1/P2 patterns above flat and discontinuous ground. Slope of section A is $\alpha_1 \simeq -1.5^{o}$ ($x_1 = 600'$, $z_1 = -15'$).

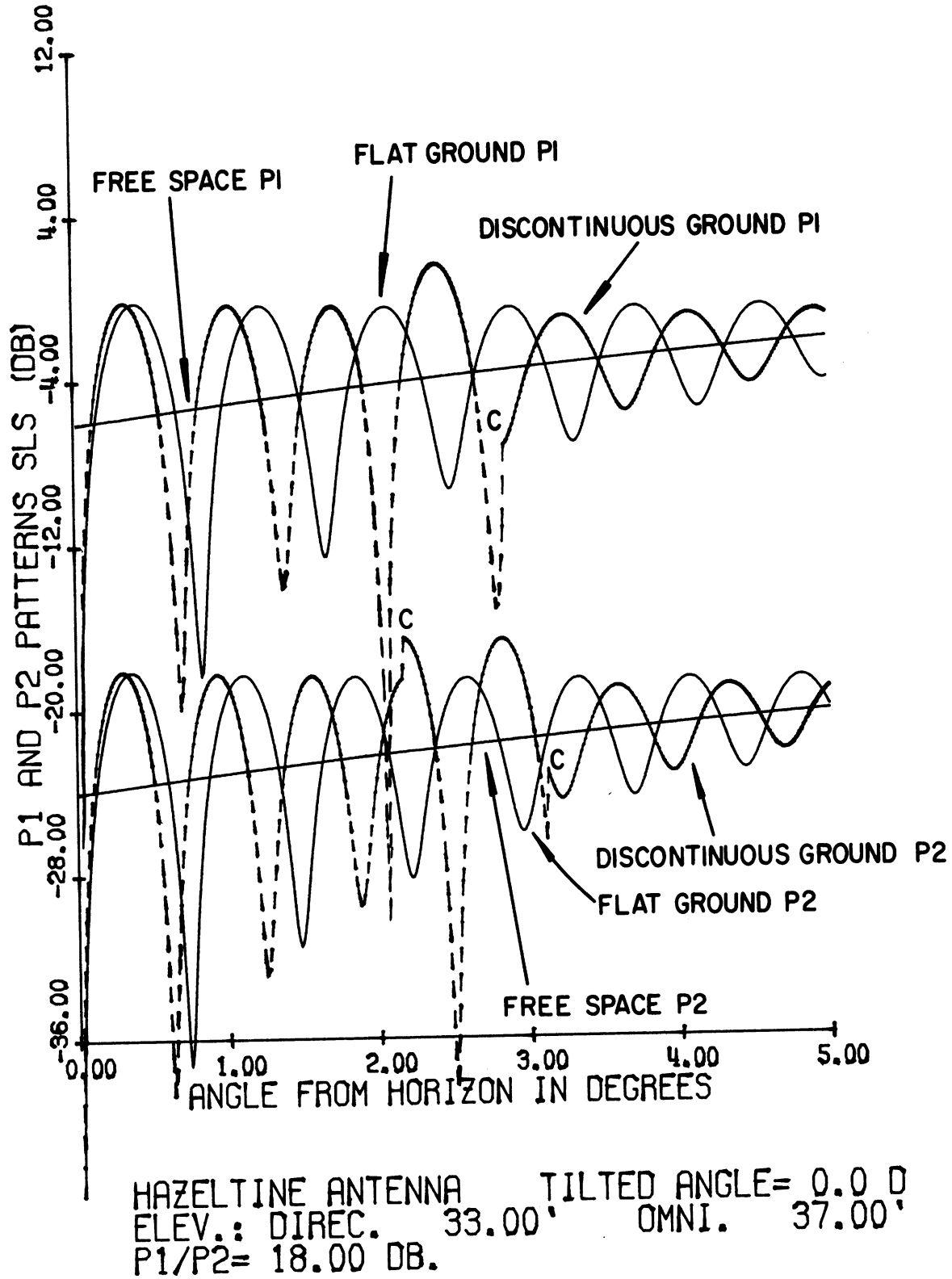

FIG. 27: P1 and P2 pulse patterns in free space and above flat and discontinuous ground. Slope of section A is $\alpha_1 \simeq -0.5^o$ ($x_1 = 800'$, $z_1 = -6.7'$).

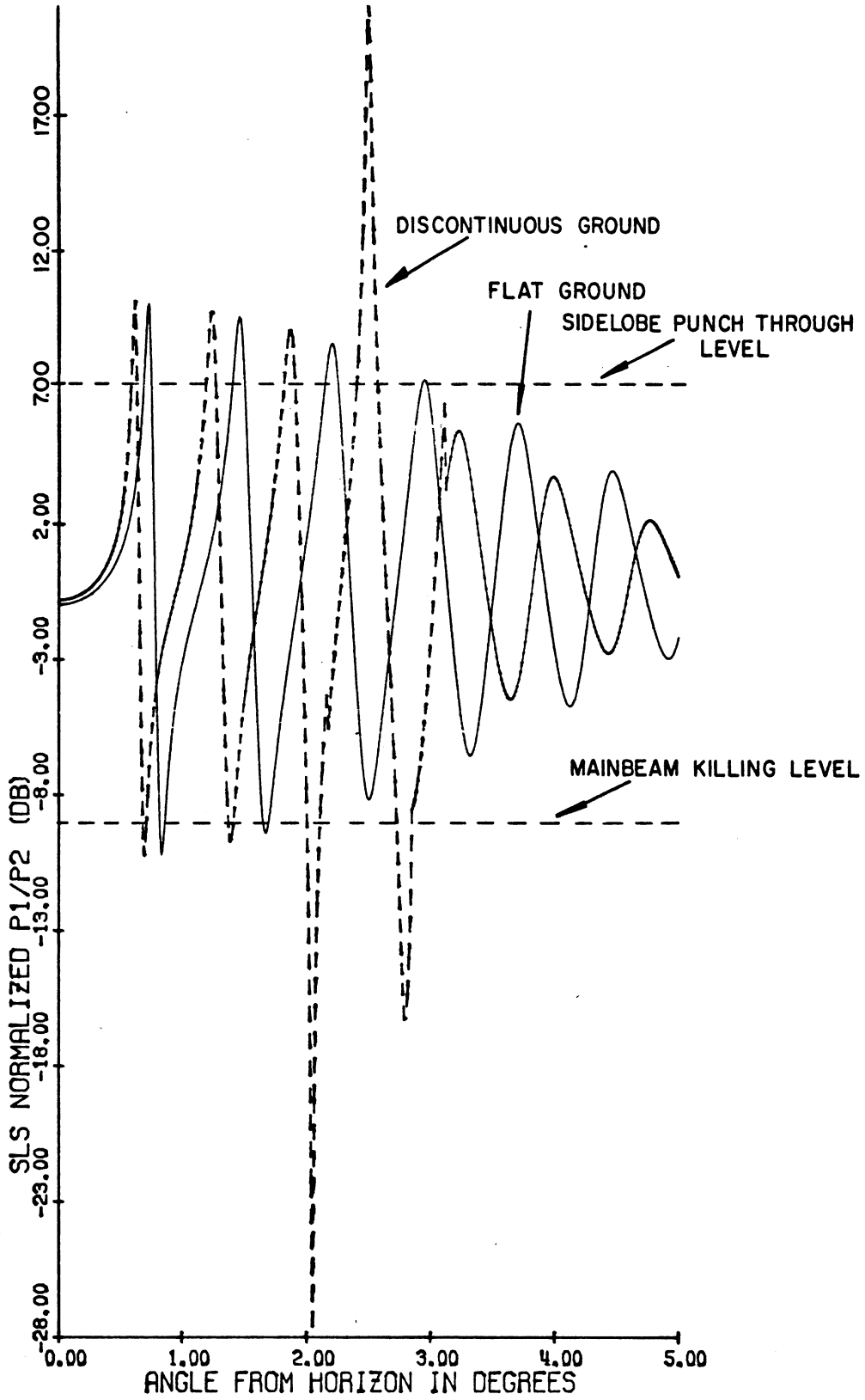

FIG. 28: P1/P2 pulse patterns above flat and discontinuous ground. Slope of section A is $\alpha_1 \simeq -0.5^{\circ}$ ($x_1 = 800'$, $z_1 = -6.7'$).

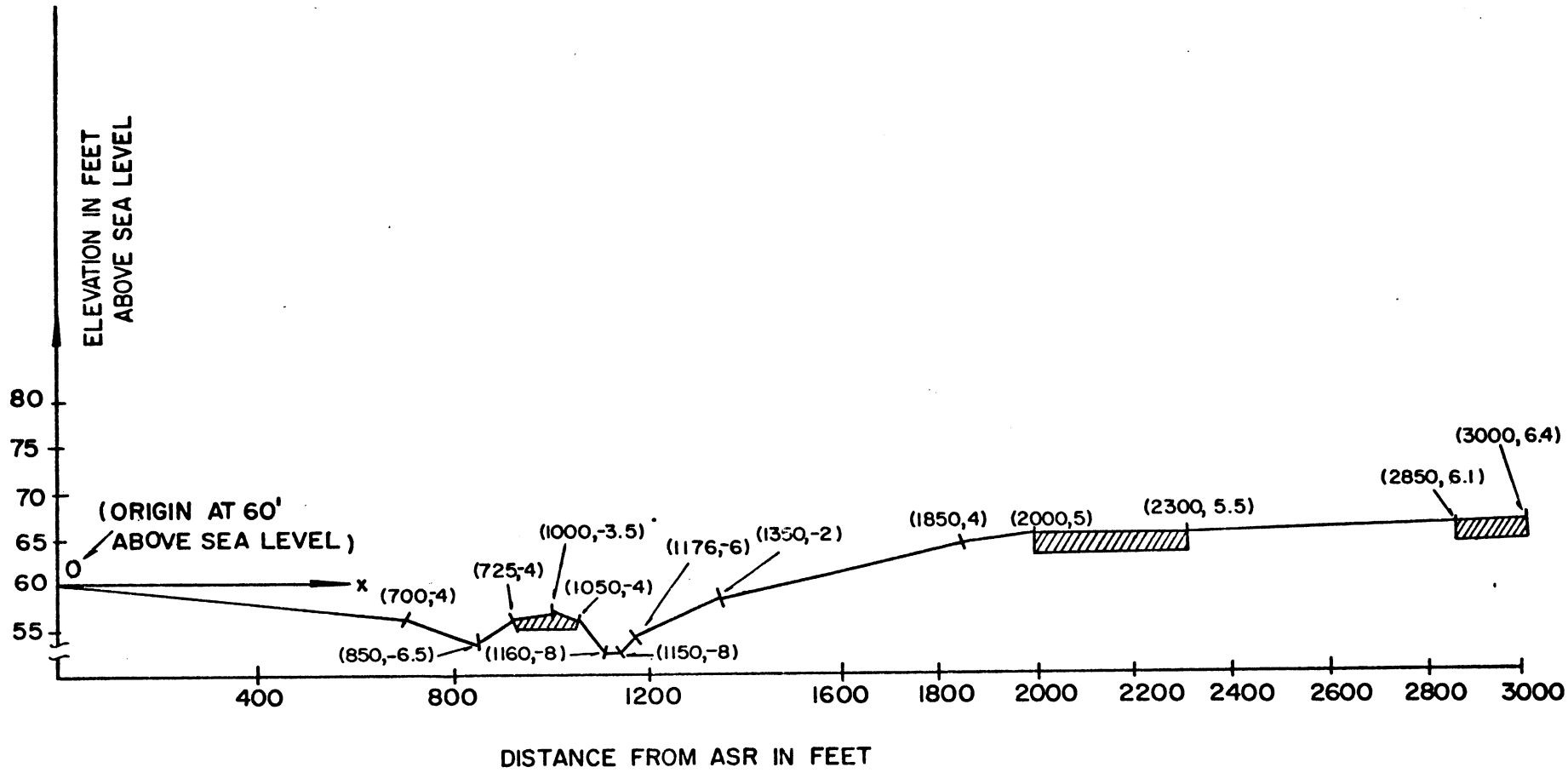

FIG. 29: NAFEC ground profile along 305° radial. Coordinates marked on the graph are with respect to the origin as shown.

MISSING
PAGE

profile reduces the depth of the first minimum but increases those of the minima at larger angles. In particular, the pattern develops a large minimum at $\theta \sim 3^{o}$ where the flat earth case had a maximum. Figure 31 results indicate that in the flat earth case there exist the mainbeam killing zones at $\theta \sim 0.9^{o}$ and 1.7^{o} and in the NAFEC profile case there exists one strong mainbeam killing zone at $\theta \sim 3^{o}$. As discussed earlier, the NAFEC profile results coincide with the free space results in the shadow regions.

Figures 32 and 33 show the effective azimuth and the number of replies, respectively, for the flat earth and NAFEC profile cases. The main effects of the NAFEC profile are found to be the removal of the zero effective azimuth beamwidth (and zero number of replies) at $\theta \sim 0.9^{o}$ and 1.7^{o} and the generation of a zone of zero effective beamwidth (zero number of replies) at $\theta \sim 3^{o}$. This may or may not be of some advantage.

Figures 34(a) and 34(b) compare the theoretical P1 pulse and amplitude results with the results obtained from inbound and outbound radial flight tests carried out at the NAFEC area. The test results were obtained when the aircraft was flying at a constant height (2000' above sea level) and along a chosen radial (305^{o}) to and from the ATCRBS. The flight test data were obtained as P1 pulse amplitude in dB as a function of the slant range of the aircraft. The measured results in Figs. 34(a) and (b) were obtained from the flight test data after removing the slant range dependency from the results and expressing them as functions of the elevation angle. Considering the various approximations made in the theory, the agreement between the measured and theoretical results shown in Figs. 34(a) and (b) may be considered to be fair. In particular, the locations of some of the maxima and minima and some finer details of the patterns are predicted very well by the theory. In the region AA and BB (of Fig. 18), the theoretical results follow the free space curve; it is believed that in these regions the agreement with measured results may be improved by considering in the theory the diffraction effects of the appropriate regions of the ground profile.

MISSING PAGE

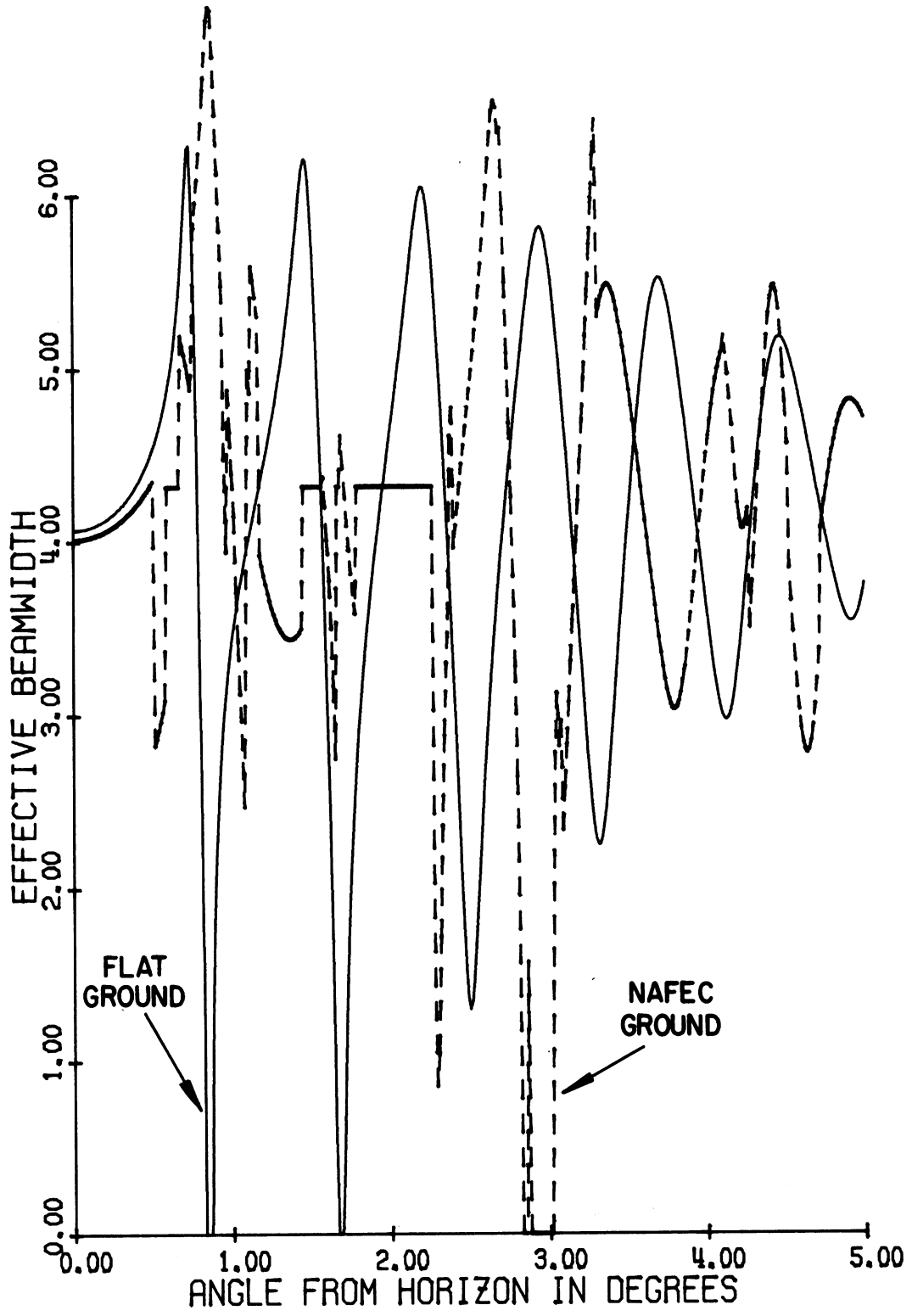

FIG. 32: Effective azimuth beamwidth as a function of θ.

MISSING
PAGE

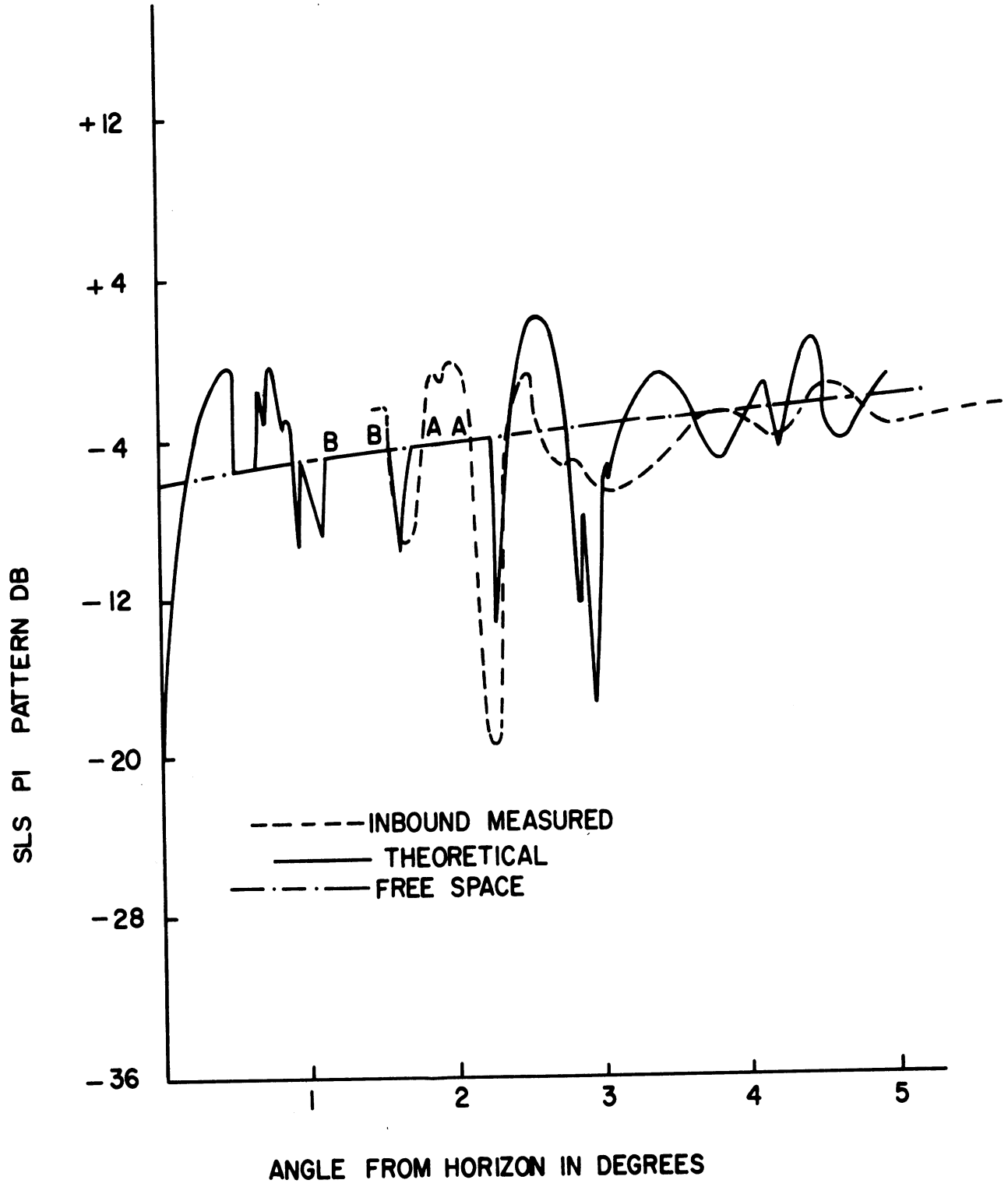

FIG. 34(a): Results for 305° radial flight at 2000' above sea level.

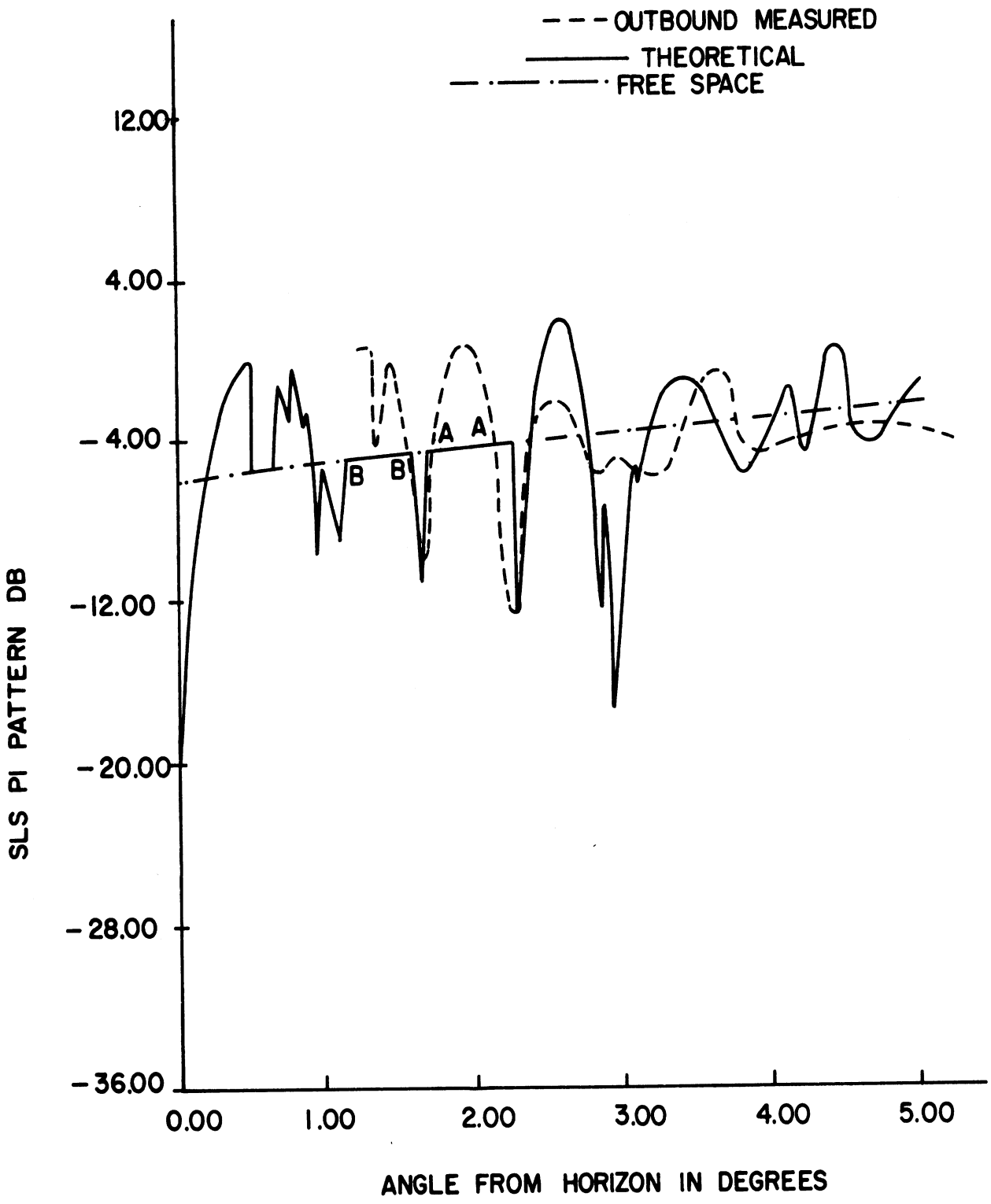

FIG. 34(b): Results for 305^{o} radial flight at 2000' above sea level.

It was mentioned earlier that during flight tests the P1 pulse amplitude data were collected as a function of the slant range of the aircraft from the ATCRBS. It may therefore be found convenient to compare the measured data directly with the theoretical results if the latter are expressed as functions of the slant range rather than the elevation angle, as was done before. Figures 35(a) and 35(b) compare the inbound and outbound measured results with the theoretical results as functions of the slant range for the ATCRBS using the Hazeltine open array antenna. The strong minimum at the slant range of approximately 6.4 nautical miles predicted by the theory appears to be missing in the measured data although it does show a minimum at that range. Figure 36 shows similar theoretical results for the flight tests with an ATCRBS using the existing Hog-Trough antenna. At the time of writing this report, no measured data are available for this case.

On the basis of the results discussed in this section, it may be said that the method developed to obtain the effects of terrain profile can predict the overall performance of ATCRBS fairly well. It may also enable one to identify the terrain sources producing some undesirable effects.

MISSING
PAGE

MISSING PAGE

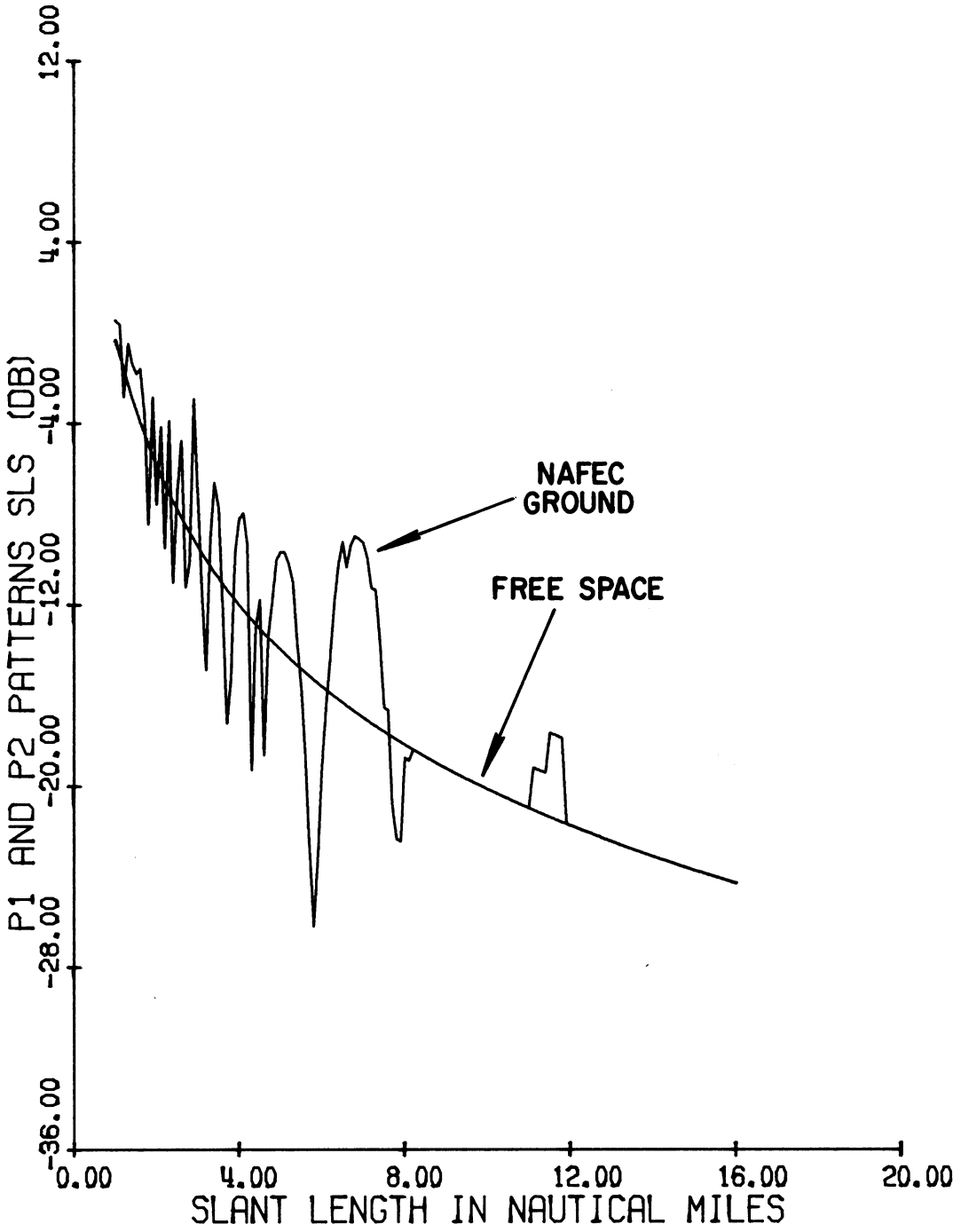

EXISTING ANTENNA TILTED ANGLE= 0.0 D
ELEV.: DIREC. 31.50' OMNI. 33.00'
P1/P2= 18.00 DB.

FIG. 36: Theoretical P1 pulse amplitude patterns as functions of the slant range for the existing Hog-Trough antenna.

5. CONCLUSIONS

Basic theoretical expressions necessary to obtain the effects of various ground profiles on the SLS mode performance of an ATCRBS have been derived. The theory is based on ray optics and neglects any effects of diffraction. Focussing effects of concave cylindrical surfaces are found to be important in regions very close to the horizon. Hence it is believed that such effects will not be of significance for normal ATCRBS operation.

Based on these theoretical formulations a computer program has been developed to obtain numerical results for ATCRBS using various antenna systems located above a ground with a specified profile. It is assumed that the ground consists of planar sections having arbitrary dielectric constant. The computer program is capable of handling any given ground profile as long as it can be approximated by planar sections. The effects of discontinuities at the junctions of the two sections are neglected.

Some representative results have been discussed for a simple case of a ground consisting of two planar sections. The results indicate that for such cases, there exists a transition region in space where the pulse and pulse ratio patterns go through strong oscillations. These oscillations may cause more severe mainbeam killing and sidelobe punch-through problems in the transition zone. The location and extent of the transition zone depend on the interrogator antenna height and on the slopes of the ground plane sections.

The performance of an ATCRBS located at NAFEC has been studied theoretically by assuming a ground profile typical of the NAFEC area. Theoretical results have been compared with those obtained from actual flight tests. The agreement obtained between theory and experiment indicates that the computer program can be used to assess the performance of ATCRBS located above a ground of given profile.

6. REFERENCES

[1] Zatkalik, J., D.L. Sengupta and C.T. Tai, "Side Lobe Suppression Mode Performance of ATCRBS with Various Antennas", FAA-RD-75-31, May 1975.

[2] Sengupta, D.L., J. Zatkalik and C.T. Tai, "Improved Side Lobe Suppression Mode Performance of ATCRBS with Various Antennas", FAA-RD-75-32, May 1975.

[3] Kerr, D.E., Propagation of Short Radio Waves , Boston Technical Publishers, Inc., Boston, Massachusetts, 1964, Chapter 5.

APPENDIX A
RAYS REFLECTED FROM CYLINDRICAL SURFACES

A.1 Introduction

In order to estimate quantitatively the field reflected from a concave or convex surface, we shall take a section of this surface, with radius of curvature a, and approximate this surface as a part of a cylinder of radius a. Therefore, in this appendix, we shall discuss the rays reflected from convex and concave cylinders, with particular interest in the divergence of reflected rays in the far zone, and the location of the caustics in the case of a convex cylinder. Parts of the results, such as the divergence factor, etc., are well known; other parts, such as the location of the caustic of a convex surface (with arbitrary direction of incidence), cannot be found explicitly in existing literature. The purpose of this appendix is to give a simple and unified derivation of these results that are used in the main text.

A.2 Reflection from a Cylinder

The reflection of rays from an antenna T by a cylinder is illustrated in Fig. A-1. Since we are interested in rays in a plane perpendicular to the axis of the cylinder, Fig. A-1 shows the plane passing through the transmitter and perpendicular to the cylinder. In this plane, we can denote any position by a complex number and any direction by a complex number with modulus unity. As illustrated in

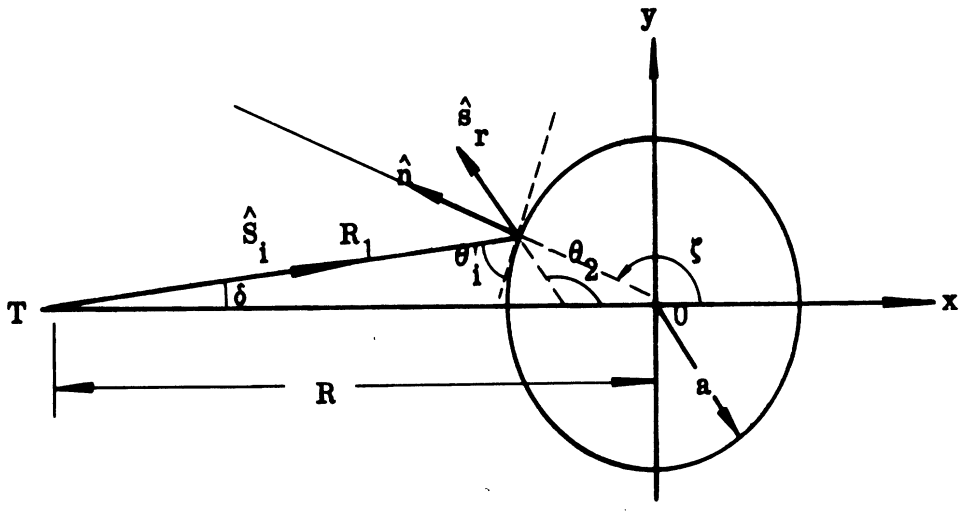

FIG. A-1: Reflection of rays from a cylinder.

Fig. A-1, we choose the axis of the cylinder 0 as the origin, and the transmitter is located at $R e^{-j\pi}$. A ray in the direction

$$\hat{s}_i = e^{j\delta}$$

is reflected at a point $a e^{j\zeta}$ on the cylinder. It is obvious that δ and ζ are related by

$$\tan\delta = \frac{a \sin\zeta}{R + a\cos\zeta} \tag{A-1}$$

For computational purposes we shall denote

$$\delta' \triangleq \frac{d\delta}{d\zeta} = \frac{(R\cos\zeta + a)}{R^2 + a^2 + 2aR\cos\zeta} = \frac{a(R\cos\zeta + R)}{R_1^2} \tag{A-2}$$

where

$$R_1 = \sqrt{R^2 + a^2 + 2aR\cos\zeta} \tag{A-3}$$

is the distance from the source T to the point of reflection. From the figure, we also see that the angle of incidence (the angle between the incident ray and the tangent plane at the point of reflection) is

$$\theta_i' = \zeta - \pi/2 - \delta \ . \tag{A-4}$$

Moreover,

$$(a + R\cos\zeta) = -R_1 \cos(\theta_i' - \frac{\pi}{2}) = -R_1 \sin\theta_i' \ .$$

Thus, we may also write Eq. (A-2) as

$$\delta' = \frac{-a\sin\theta_i'}{R_1} \ . \tag{A-5}$$

The direction of the reflected ray is given by

$$\hat{s}_r = e^{i\theta_r} \tag{A-6}$$

where

$$\theta_r = 2\theta_i' + \delta = 2\zeta - \pi - \delta \ . \tag{A-7}$$

Thus, if we denote t as the distance measured along the reflected ray from the point of reflection, any point on the reflected ray may be expressed in the parametric form

$$x+jy = a e^{i\zeta} + t e^{j\theta_r} = a e^{j\zeta} - t e^{j2\zeta - \delta} \ . \tag{A-8}$$

Now let us consider an adjacent ray in the direction $e^{j\delta + d\delta}$, and reflected from the point $a e^{j(\zeta + d\zeta)}$, then, any point on this reflected ray may be expressed in the parametric form

$$x+jy = a e^{j(\zeta+d\zeta)} - \tilde{t} e^{j(2\zeta - \delta)} e^{j(2d\zeta - d\delta)}$$

$$= a e^{j\zeta} e^{jd\zeta} - \tilde{t} e^{j(2\zeta - \delta)} e^{j(2\zeta - \delta)} e^{j(2 - \delta')d\zeta} \tag{A-9}$$

where $\tilde{t}$ is the distance measured along the adjacent reflected ray from its point of reflection. The values of t and $\tilde{t}$ at the point of intersection of the two adjacent reflected rays may be obtained by equating Eqs. (A-8) and (A-9). To the first power of $d\zeta$, we have

$$\tilde{t} - t = jd\zeta \left[a e^{-j(\zeta - \delta)} - (2 - \delta')\tilde{t} \right] \ . \tag{A-10}$$

Since both t and $\tilde{t}$ must be real, we conclude from Eq. (A-10) that as $d\zeta \longrightarrow 0$ (the two adjacent reflected rays are very close to each other),

$$t \cong \tilde{t} = \frac{a\cos(\zeta - \delta)}{(2 - \delta')} \quad . \tag{A-11}$$

Introducing Eq. s (A-4) and (A-5) into (A-11) yields

$$t = - \frac{aR_1 \sin\theta_i}{2R_1 + a\sin\theta_i} \tag{A-12}$$

From Eq. (A-12), we see that t is negative, indicating that the rays form a "virtual image" at a distance

$$f = |t| = \frac{aR_1 \sin\theta_i'}{2R_1 + a\sin\theta_i} \tag{A-13}$$

behind the point of reflection.

In terms of f, it is easy to deduce the conventionally used "divergence factor" by referring to Fig. A-2. In A-2(a), it is seen that the two adjacent rays reflected from a convex cylindrical surface intersect a distance f behind the point of reflection. In Fig. A-2(b), it is seen that for the same incident rays, the adjacent reflected rays from the tangent plane intersect at a distance R_1 behind the point of reflection. Thus, the the same amount of incident power, the reflected rays from the cylinder have an angular spread $\Delta\psi_c$ while the angular spread of rays reflected from the tangent plane is $\Delta\psi_p$ and

$$\frac{\Delta\psi_p}{\Delta\psi_c} = \frac{f}{R_1} \tag{A-14}$$

Therefore, the magnitude of the field reflected by a convex cylindrical surface of radius of curvature a may be obtained from the field reflected from the tangent plane multiplied by the divergence factor

$$D = \sqrt{\frac{\Delta\psi_p}{\Delta\psi_c}} = \sqrt{\frac{f}{R_1}} = \sqrt{\frac{a\sin\theta_i'}{2R_1 + a\sin\theta_i'}} \tag{A-15}$$

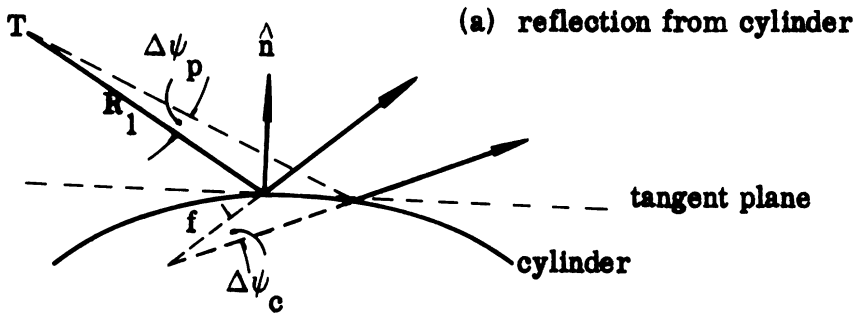

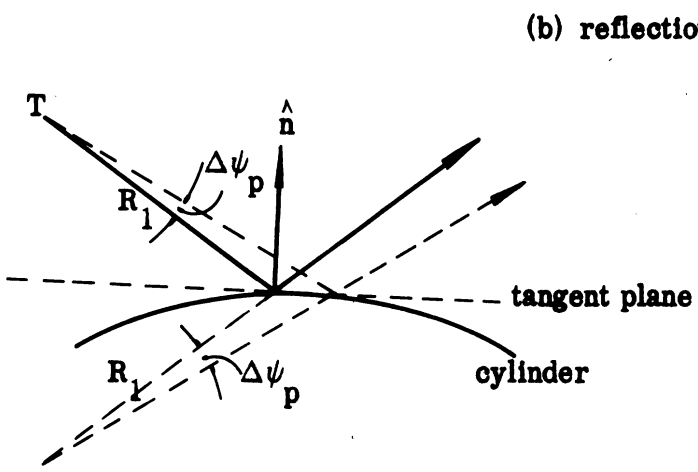

FIG. A-2: Reflections from convex surfaces.

A.3 Reflection from Concave Cylindrical Surfaces

The reflection of rays from a concave cylindrical surface can be analyzed in the same procedure as used for the case of the convex cylinder. As illustrated

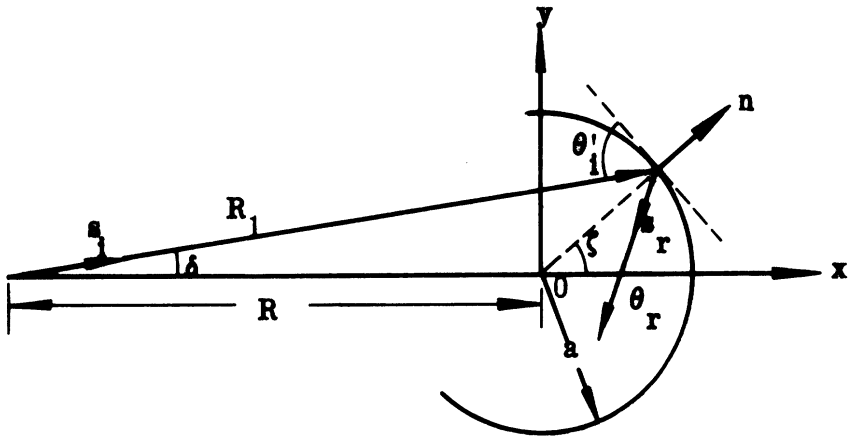

FIG. A-3: Reflection from a concave cylindrical surface.

in Fig. A-3, an incident ray in the direction

$$\hat{s}_i = e^{j\delta} \tag{A-16}$$

is reflected from a point $a e^{j\zeta}$. The relation between δ and ζ is

$$\tan\delta = \frac{a \sin\zeta}{R + a\cos\zeta} \quad ; \tag{A-17}$$

therefore,

$$\delta' \triangleq \frac{d\delta}{d\zeta} \frac{a(a+R\cos\zeta)}{R^2+a^2+2aR\cos\zeta} = \frac{a(a+R\cos\zeta)}{R_1^2} \tag{A-18}$$

where

$$R_1 = \sqrt{R^2+a^2+2aR\cos\zeta} \tag{A-19}$$

is the distance from the transmitter T to the point of reflection. The "angle of incidence" is given by

$$\theta_i' = \frac{\pi}{2} - \zeta + \delta \tag{A-20}$$

since

$$a + R\cos\zeta = R_1 \cos\theta_i' = R_1 \sin\theta_i' \quad .$$

Equation (A-18) may also be written as

$$\delta' = \frac{a \sin\theta_i'}{R_1} \tag{A-21}$$

The direction of the reflected ray is

$$\hat{s}_r = e^{j\theta_r} \tag{A-22}$$

where

$$\theta_r = -(\pi - 2\zeta + \delta) \quad . \tag{A-23}$$

Therefore any point on the reflected ray may be represented in the parametric form

$$x + jy = a e^{i\zeta} - t e^{j(2\zeta - \delta)} \tag{A-24}$$

where t is the distance measured along the reflected fay from the point of reflection. Similarly, from an adjacent ray with incident direction $e^{j(\delta + d\delta)}$, reflected at a point $a e^{j(\zeta + d\zeta)}$, any point on this adjacent reflected ray may be expressed in the parametric form

$$x + jy = a e^{j(\zeta + d\zeta)} - \tilde{t} e^{j(2\zeta - \delta)} e^{j(2 - \delta')_{d\zeta}} \tag{A-25}$$

where $\tilde{t}$ is the distance measured along the adjacent reflected ray from its point of reflection. The values of t and $\tilde{t}$ at the point of intersection of the two adjacent rays may be obtained by equating Eqs. (A-24) and (A-25). To the first power of $d\zeta$ we have

$$\tilde{t} - t = \left[a e^{-j(\zeta - \delta)} - t(2 - \delta')\right] j d\zeta \quad . \tag{A-26}$$

Since t and $\tilde{t}$ are both real, we conclude that for $d\zeta \rightarrow 0$,

$$t = \tilde{t} = \frac{a\cos(\zeta - \delta)}{2 - \delta} = \frac{R_1 a \sin\theta_i'}{2R_1 - a\sin\theta_i'} \quad . \tag{A-27}$$

For the reflection of rays from concave surfaces, we therefore have two cases, depending on the sign of t in Eq. (A-27). Again let us define

$$f = |t| \quad , \tag{A-28}$$

then for the case $t < 0$, the reflected ray diverges, as illustrated in Fig. A-4(a). For this case, it is obvious that the divergence factor introduced in Section A.2, i.e.,

$$D = \sqrt{f/R_1} \tag{A-29}$$

can be applied. On the other hand, when $t > 0$, the reflected rays converge to a caustic as illustrated in Fig. A-4(b). For this case the field strength at and near the caustic becomes very large, and in general cannot be predicted by ray theory. However, if we assume that for the far field our observation point is very far from the reflection point f, then again the rays are divergent, and the use of the divergence factor defined by Eq. (A-29) is appropriate.

To test whether it is appropriate to use the divergence factor and ray theory in computing the reflected field at any point, it would be necessary to find the location of the caustic and make sure that the point of interest is far away from the caustic. To find the location of the caustic, let us denote the direction of the incident ray by $e^{-j\theta_i}$, and that of the reflected ray by $e^{j\theta}$; then, corresponding to a given θ_i, the location of the caustic region is given by

$$x_c = R_1\cos\theta_i + f\cos\theta \tag{A-30}$$

$$z_c = H - R_1\sin\theta_i + f\sin\theta \tag{A-31}$$

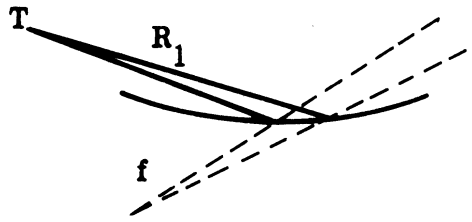

FIG. A-4(a): **Divergent rays reflected from concave cylinder.**

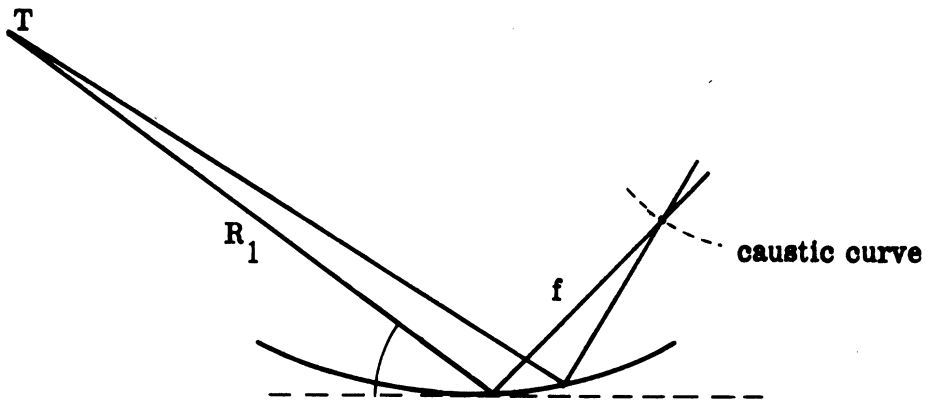

FIG. A-4(a): **Convergent rays reflected from concave cylinder.**

where H is the height of the antenna. Thus, for our purpose, if the fields are to be computed at points with $z \gg z_c$, then ray theory can be used to compute the field pattern.

APPENDIX B
COMPUTER PROGRAM
FOR CALCULATING THE GROUND PROFILE EFFECTS

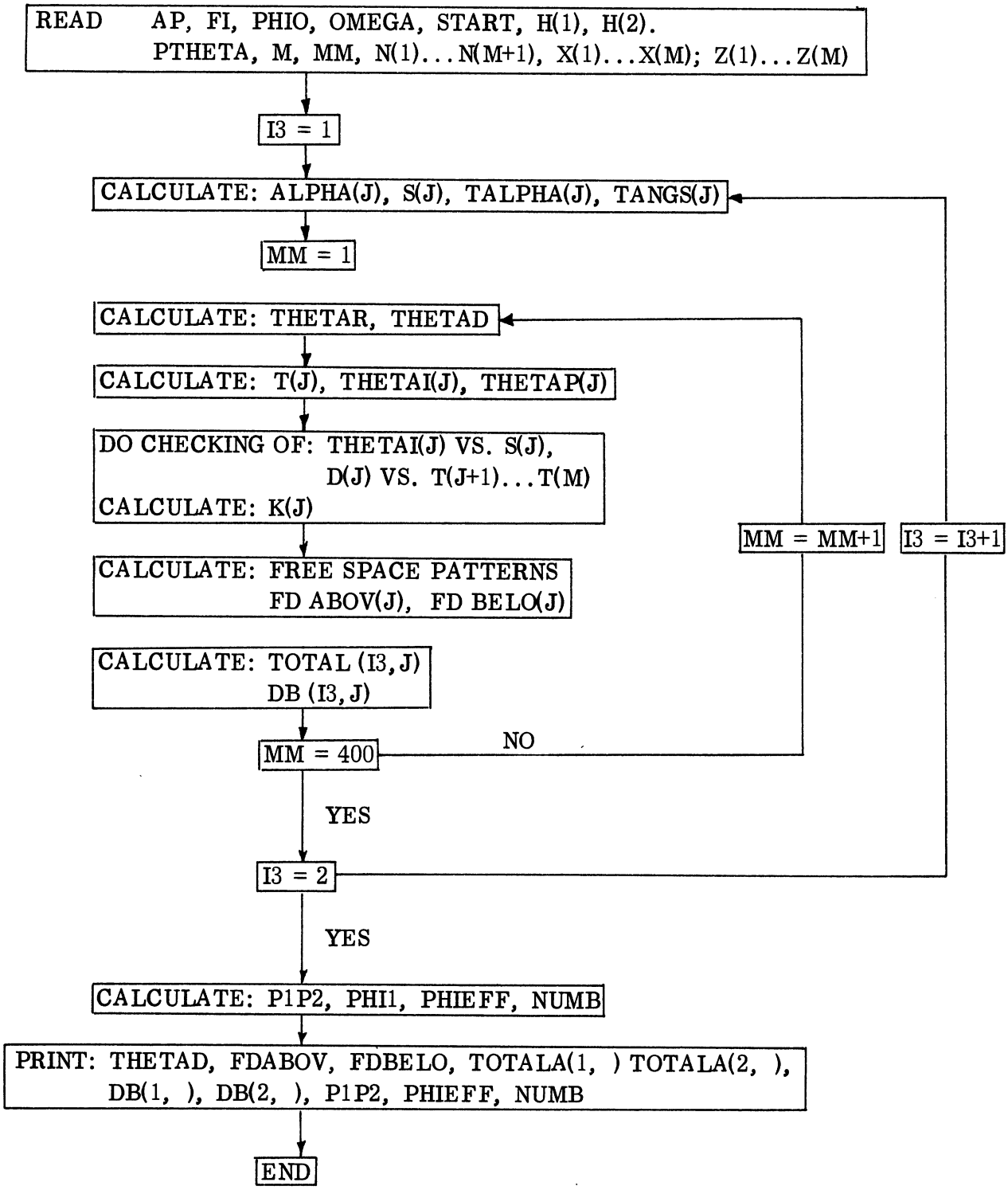

FIG. A-1: Flow chart for main program.

List of Symbols for Main Program

ALPHA(M+1) = α_{m+1}

ALPHA(J) = α_j

CABS = absolute value (complex)

DB(1, I) = 20 log 10 TOTALA(1, I)

DB(2, I) = 20 log 10 TOTALA(2, I)

DELTA(J) = Δ_j

D(J) = D_j

FDABOV = Fd(θ)

FDBELO = Fd(-θ)

HP(J) = HP_j

K(J) = K_j

NUM = number of replies

P(J) = ρ_j

PHIEFF = effective beamwidth

P1P2 = normalized P1/P2

S(J) = S_j

SQRT = square root

THETAI(J) = ϑI_j

THETAP(J) = θP_j

THETAD = θ in degrees

THETAR = θ in radians

THETAM = -θ

T(J) = T_j

TOTALA(1, I) = P1(θ) SLS

TOTALA(2, I) = P2(θ) SLS

Main Program

```
C**********************************************************************
C     THE EFFECTS OF GROUND PROFILES ON THE AIRBS PERFORMANCE
C
C       GLOSSARY OF NAMES USED FOR THE INPUT QUANTITIES
C
C       AP        ANTENNA  TYPE:
C                 1 WESTINGHOUSE ANTENNA
C                 2 TEXAS INSTRUMENTS ANTENNA
C                 3 HAZELTINE ANTENNA
C                 4 EXISTING ANTENNA
C                 5 NADIF FIX1 ANTENNA
C                 6 TEXAS FIX ANTENNA
C                 7 HAZELTINE ESCAN ANTENNA
C       BETA      FREE SPACE PROPAGATION CONSTANT
C       DTHETA    INCREMENTAL VALUE OF THETA
C       FI        INTERROGATOR PULSE REPETITION
C       H(1)      HEIGHT OF THE DIRECTIONAL ANTENNA
C       H(2)      HEIGHT OF THE OMNIDIRECTIONAL ANTENNA
C       N(I)      INDEX OF REFRACTION FOR GROUND SECTION I
C       M         NUMBER OF GROUND SECTIONS
C       MM        NUMBER OF POINTS TO BE COMPUTED
C       OMEGA     ANGULAR SCANNING RATE (DEG./SEC.)
C       PHIO      TOTAL HALF-POWER BEAMWIDTH OF THE AZIMUTHAL PATTERN OF THE
C                 DIRECTIONAL ANTENNA
C       START     INITIAL THETA VALUE (DEG.)
C       X(I)      HORIZONTAL DISTANCE TO POINT I
C       Z(I)      VERTICAL DISTANCE TO POINT I
C**********************************************************************
      INTEGER AP
      REAL N(20)
      COMPLEX ARG2A,K,SUM,TOTAL
      DIMENSION X(20),Z(20),ALPHA(20),TALPHA(20),THETAI(20),
     *HP(20),THETAP(20),TANGS(20),S(20),I(20),DELTA(20),K(20),D(20),
     *P(20),H(2),DB(2,400),THETAD(400)
     *,EDABOV(400),EDBELO(400),
     *TOTALA(2,400)
      WRITE(6,115)
C
C*****READ IN THE DATA
C
      READ(5,100) AP,FI,PHIO,OMEGA,START,H(1),H(2),BETA,DTHETA,M,MM
      M1=M+1
      READ(5,101,END=1)  (N(I),I=1,M1)
    1 READ(5,101,END=2)  (X(I),I=1,M)
    2 READ(5,101,END=3)  (Z(I),I=1,M)
C
C*****LOOP FOR DOING THE DIRECTIONAL AND OMNIDIRECTIONAL ANTENNAS
C*****(P1 AND P2 PULSES,BOTH IN DB AND ABSOLUTE VALUE)
C
    3 DO 59 I3=1,2
      WRITE(6,108)
```

```
C*****LOOP FOR COMPUTING THE ALPHA'S,TALPHA'S,HP'S,TANGS'S,S'S
C
      ALPHA(M+1)=0.0
      HP(M+1)=H(I3)-Z(M)
      S(M+1)=0.0
      DO 9 J=1,M
      IF (J .NE. 1) GO TO 5
      TALPHA(J)=Z(J)/X(J)
      ALPHA(J)=ATAN2(Z(J),X(J))
      HP(J)=H(I3)
      GO TO 7
    5 TALPHA(J)=(Z(J)-Z(J-1))/(X(J)-X(J-1))
      ALPHA(J)=ATAN2(Z(J)-Z(J-1),X(J)-X(J-1))
      HP(J)=H(I3)-Z(J-1)+X(J-1)*TALPHA(J)
    7 TANGS(J)=(H(I3)-Z(J))/X(J)
      S(J)=ATAN2(H(I3)-Z(J),X(J))
    9 CONTINUE
C
C*****LOOP FOR RUNNING THETA FROM X TO Y DEGREES
C
      DO 99 I=1,MM
C*****CONVERT TO RADIANS
      THETAR=(START+DTHETA*I)*3.14159265/180.0
      THETAD(I)=I*DTHETA+START
      WRITE(9,102) THETAD(I),THETAR
C
C*****LOOP FOR COMPUTING ALL THE T'S,THETAI'S,THETAP'S
C
      DO 19 J=1,M1
      T(J)=X(J)*(TAN(THETAR))-Z(J)
      THETAI(J)=THETAR-2.0*ALPHA(J)
   19 THETAR(J)=THETAR-ALPHA(J)
C
C*****LOOP FOR EVALUATING THE K'S
C
      DO 29 J=1,M1
C
C*****FIRST CHECK: COMPARISON OF THETAI(J) WITH THE S'S;
C                  IF THETAI(J) < S(J) OR IF THETAI(J) > S(J-1)...S(1)
C                  SET K(J)=0; OTHERWISE CONTINUE TO NEXT CHECK
C
C*****FIRST CASE IS SPECIAL: IF THETAI(1) < S(1) SET K(1)=0;
C                            OTHERWISE CONTINUE TO NEXT CHECK
       IF(J .NE. 1) GO TO 22
      IF(THETAI(J) .LT.S(J)) GO TO 28
      GO TO 29
   22 IF (THETAI(J) .LE. S(J)) GO TO 28
      JJ=J-1
   24 IF (THETAI(J) .GT. S(JJ)) GO TO 28
      IF (JJ .EQ. 1) GO TO 26
      JJ=JJ-1
      GO TO 24
```

```
C*****NEXT CHECK: EVALUATE D(J) AND COMPARE IT WITH T(J+1)...T(M);
C                 IF IT IS GREATER THAN ALL OF THESE T'S; SET K(J)=0;
C                 OTHERWISE, COMPUTE DELTA(J) AND P(J) AND USE THESE TO
C                 COMPUTE K(J).
C                 IF J IS GREATER THAN OR EQUAL TO M,DON'T
C                 CHECK; JUST EVALUATE K.
C
   26 D1=HP(J)*(TAN(THETAI(J))+TAN(THETAP))
      D2=TAN(THETAI(J))+TALPHA(J)
      D(J)=D1/D2-H(I3)
      JJ=J+1
      IF(J.GE.M) GO TO 32
      DO 39 II=JJ,M
      IF(D(J) .GT. T(II)) GO TO 39
   32 DELTA(J)=2.0*HP(J)*COS(ALPHA(J))*SIN(THETAP(J))
      P1=N(J)**2*SIN(THETAP(J))
      P2=SQRT(N(J)**2-1.0+(SIN(THETAP(J)))**2)
      P(J)=(P1-P2)/(P1+P2)
      ARG1=DELTA(J)*BETA*(-1.0)
      ARG2A=CMPLX(0.0,ARG1)
      K(J)=P(J)*CEXP(ARG2A)
      GO TO 30
   39 CONTINUE
   28 K(J)=CMPLX(0.0,0.0)
   30 WRITE(9,103)J,THETAI(J),J,K(J)
   29 CONTINUE
C
C*****CALCULATION OF FREE SPACE POINTS
C
      FD1=0.0
      SUM=CMPLX(0.0,0.0)
C*****CALCULATE FREE SPACE PATTERNS FOR ABOVE AND BELOW THE HORIZON
      IF(I3.EQ.2) GO TO 40
      THETAM=-THETAR
      CALL FSP(FDABOV(I),AP,THETAR)
      CALL FSP(FDBELO(I),AP,THETAM)
      IF (FDBELO(I) .LE. -36.0) FDBELO(I)=-36.0
C
C*****LOOP FOR CALCULATING FREE SPACE PATTERN FOR -THETAI'S THAT HAVE
C     CORRESPONDING NON-ZERO K'S
C
   40 DO 49 L=1,M1
      IF(REAL(K(L)) .EQ. 0.0 .AND. AIMAG(K(L)) .EQ. 0.0) GO TO 49
      THETAS=-THETAI(I)
      CALL FSP(FD1,AP,THETAS)
      SUM=SUM+FD1*K(L)
   49 CONTINUE
      TOTAL=FDABOV(I)+SUM
      TOTALR=REAL(TOTAL)
      TOTALI=AIMAG(TOTAL)
      TOTALA(I3,I)=CABS(TOTAL)
      DP(I3,I)=20.0*ALOG10(TOTALA(I3,I))-(I3-1.0)*18.0
   50 CONTINUE
```

```
C*****CALCULATION OF P1/P2 PULSE (SLS),EFFECTIVE BEAMWIDTH, AND
C*****THE NUMBER OF REPLIES
C
       DO 69 I=1,MM
      P1P2=DB(1,I)-DB(2,I)-18.0
      PHI1=(DB(1,I)-DB(2,I)-9.0)/12.0735
      IF (PHI1 .LE. 0.0) GO TO 65
      PHIEFF=2.0*PHI0*SQRT(PHI1)
       GO TO 67
   65 PHIEFF=0.0
   67 NUMB=FI*PHIEFF/OMEGA
C
C*****NOW PRINT OUT EVERYTHING ONTO ONE UNIT
C
   69 WRITE(6,110)THETAD(I),FDABOV(I),FDBELO(I),TOTALA(1,I),TOTALA(2,I)
     *,DB(1,I),DB(2,I),P1P2,PHIEFF,NUMB
C
C*****THE FORMAT STATEMENTS
C
  100 FORMAT(I2,8F12.6,2I4)
  101 FORMAT(5F12.6)
  102 FORMAT(' FOR THETA=',F8.4,F12.6)
  103 FORMAT(T1,' ',T20,'THETAI(',I2,') =',F12.6,T50,'K(',I2,
     *')=',2F12.6)
  108 FORMAT('1')
  110 FORMAT(F8.4,8(F14.4),3X,I3)
  115 FORMAT('1 THETA',5X,'ABOVE HOR.',4X,'BELOW HOR.   P1 PULSE SLS',
     *'  P2 PULSE SLS',3X,'P1 SLS DB',5X,'P2 SLS DB',4X,'P1P2 SLS DB'
     *,4X,'EFF.  BEAM NO OF REP'//)
      END



      SUBROUTINE FSP(ANSWER,AP,ANGLE)
      INTEGER AP
      DIMENSION A(7),C(15,7)
      DATA A /4.3738,1.7039,0.4554,1.1086,0.2644,0.6346,0.8108/
      DATA C/-64.85,-135.06,13.02,-64.65,-151.88,-47.04,-91.27,8*0.0,
     *0.084,0.080,0.500,1.000,0.800,0.860,0.790,0.860,0.960,0.540,
     *0.230,0.120,0.060,2*0.0,
     *0.500,1.000,0.885,0.530,11*0.0,
     *0.084,0.51,0.966,0.780,0.045,10*0.0,
     *0.01,0.094,0.635,0.99,0.53,0.542,0.515,0.515,0.43,0.465,0.437,
     *0.327,0.302,0.217,0.153,
     *0.01,.039,.561,.995,.482,.45,.435,.42,.355,.417,.342,.35,.334
     *,.24,.12,
     *0.079,0.072,0.03,0.53,0.915,0.945,0.845,0.845,0.315,0.034,5*0.0/
      PI=3.14159265
      DR=0.017453292
      GO TO (1,2,3,4,5,5,6),AP
```

```
C*****SET UP CONSTANTS AND THE NUMBER OF ITERATIONS FOR THE DIFFERENT
C*****ANTENNAS
C
     1 NS=7
       B=2.0*6.4*1030.0/11808.0
       GO TO 8
     2 NS=13
       K1=3
       SIN1=0.07846
       GO TO 8
     3 NS=4
       K1=1
       SIN1=0.22495
       GO TO 8
     4 NS=5
       K1=3
       SIN1=0.47767
       GO TO 8
     5 NS=15
       K1=3
       SIN1=0.0583
       GO TO 8
     6 NS=10
       K1=4
       SIN1=0.11942
     8 SINANG=SIN(ANGLE)
       ANSWER=0.0
       IF(AP .EQ. 1) GO TO 11
C*****FREE SPACE PATTERN FOR ALL EXCEPT WESTINGHOUSE ANTENNA
       ARGG=SINANG/SIN1
       DO 10 K=1,NS
       ARG=PI*(ARGG-K+K1)
       IF(ABS(ARG) .LE. 0.0349) GO TO 9
       ANSWER=ANSWER+C(K,AP)*SIN(ARG)/ARG
       GO TO 10
     9 ANSWER=ANSWER+C(K,AP)
    10 CONTINUE
       GO TO 200
C*****FREE SPACE PATTERN FOR THE WESTINGHOUSE ANTENNA
    11 COSANG=COS(ANGLE)
       ARG2=PI*COSANG/2.0
       ARG3=PI*SINANG/2.0
       ANS1=SIN(ARG2)*COS(ARG3)/COSANG
       ANSWER=5.4201*ANS1
       DO 12 K=1,NS
       ARG4=K*PI*B*SINANG
       ANSWER=ANSWER+2.0*ANS1*A(K)*COS(ARG4+DR*C(K,AP))
    12 CONTINUE
       ANSWER=ANSWER/15.686
   200 RETURN
       END
```

Program for Graphical Output. SPLOT

```
C*************************************************************************
C     GRAPHIC REPRESENTATION OF THE VALUES COMPUTED IN THE EFFECTS
C     OF GROUND PROFILES ON THE ATCRBS PERFORMANCE PROGRAM
C
C        THE OUTPUT FROM THAT PROGRAM IS USED AS INPUT FOR THIS
C        PROGRAM
C
C        BEMLVL(I)      EFFECTIVE BEAMWIDTH ON LEVEL GROUND
C        BEMNEW(I)      EFFECTIVE BEAMWIDTH ON THE ACTUAL GROUND
C        H              THE HEIGHT OF THE AIRCRAFT
C        NUMLVL(I)      NUMBER OF REPLIES ON LEVEL GROUND
C        NUMNEW(I)      NUMBER OF REPLIES ON THE ACTUAL GROUND
C        NUMPLT         NUMBER OF PLOTS THAT YOU WANT PLOTTED
C        N1             THE PLOT NUMBER
C        P1(I)          P1 PULSE FOR WORKING WITH R(I)
C        P1FRE(I)       FREE SPACE PATTERN FOR P1 FOR WORKING WITH R(I)
C        P1FREE(I)      FREE SPACE PATTERN FOR P1 PULSE
C        P1LEVL(I)      P1 PULSE ON LEVEL GROUND
C        P1NEW(I)       P1 PULSE ON THE ACTUAL GROUND
C
C        P12LVL(I)      NORMALIZED P1/P2 PATTERN ON LEVEL GROUND
C        P1P2(I)        NORMALIZED P1/P2 PATTERN ON THE ACTUAL GROUND
C        P2FREE(I)      FREE SPACE PATTERN FOR P2 PULSE
C        P2LEVL(I)      P2 PULSE ON LEVEL GROUND
C        P2NEW(I)       P2 PULSE ON THE ACTUAL GROUND
C        Q              THE ANSWER TO QUIERRIES (YES,NO)
C        R(I)           SLANT LENGTH (IN NAUTICAL MILES)
C        THETAD(I)      ANGLE FROM HORIZON (IN DEGREES)
C
C
C
C     NOTE:THIS PROGRAM USES A MTS ROUTINE (FREAD) TO READ IN DATA FROM
C          THE TERMINAL UNFORMATED. THESE CALLS TO FREAD WILL HAVE TO BE
C          REPLACED BY FORMATED READ STATEMENTS IN ORDER TO RUN ON OTHER
C          COMPUTER INSTALLATIONS THAT DO NOT HAVE THIS CAPABILITY.
C*************************************************************************
      INTEGER*4 Q,Y,N,B
      REAL NUMLVL(400),NUMNEW(400)
      DIMENSION T1(10),T2(10),T3(10),T4(10),XPRNT(10),YPRNT1(10)
      DIMENSION YPRNT2(10),THETAD(400),P1FREE(400),P2FREE(400),P1P2(400)
      DIMENSION P1LEVL(400),BEMLVL(400),P2LEVL(400),P1NEW(400),P2NEW(400)
      DIMENSION P12LVL(400),BEMNEW(400),YPRNT3(10),YPRNT4(10)
      DIMENSION P1FRE(151),XPRNT1(10),P1(151),R(151)
      DATA Y/'Y'/,N/'N'/,B/'   '/
C
C*****READ IN THE DATA
C
    9 DO 10 I=1,400
      READ(5,100) DUMMY,DUMMY,DUMMY1,DUMMY2,DUMMY3,P1LEVL(I),
     *P2LEVL(I),P12LVL(I),BEMLVL(I),NUM1
   10 NUMLVL(I)=FLOAT(NUM1)
```

```
   20 DO 30 I=1,400
      READ(6,100) THETAD(I),P1FREE(I),DUMMY3,DUMMY4,DUMMY5,P1NEW(I),
     *P2NEW(I),P1P2(I),BEMNEW(I),NUM2
      P1FREE(I)=20.0*ALOG10(P1FREE(I))
      P2FREE(I)=P1FREE(I)-18.0
   30 NUMNEW(I)=FLOAT(NUM2)
      WRITE(7,115)
      CALL FREAD(7,'R:',H)
      DO 40 I=1,151
      R(I)=0.9+0.1*I
      THETA1=ARSIN(H/(R(I)*6076))
      TH1=THETA1*180.0/3.14159265
      J=TH1/(THETAD(2)-THETAD(1))
      P1FRE(I)=P1FREE(J)-20.0*ALOG10(R(I))
   40 P1(I)=P1NEW(J)-20.0*ALOG10(R(I))
C
C*****READ IN THE TITLES
C
      READ(8,103) (T1(I),I=1,10)
      READ(8,103) (T2(I),I=1,10)
      READ(8,103) (T3(I),I=1,10)
      READ(8,103) (T4(I),I=1,10)
      READ(8,103) (XPRINT(I),I=1,10)
      READ(8,103) (YPRNT1(I),I=1,10)
      READ(8,103) (YPRNT1(I),I=1,10)
      READ(8,103) (YPRNT2(I),I=1,10)
      READ(8,103) (YPRNT3(I),I=1,10)
      READ(8,103) (YPRNT4(I),I=1,10)
  100 FORMAT(F8.4,8(E14.4),3X,I3)
  103 FORMAT(10A4)
  105 FORMAT(' HOW MANY PLOTS DO YOU WANT?')
  106 FORMAT(' ENTER PLOT NUMBER')
  107 FORMAT(' DO YOU WANT LEVEL GROUND INCLUDED?(Y,N)')
  108 FORMAT(' DO YOU WANT FREE SPACE PATTERN INCLUDED?(Y,N)')
  109 FORMAT(' INCORRECT PLOT NUMBER, TRY AGAIN')
  110 FORMAT(' PLOT NUMBERS:',/,8X,'1     P1 VS. THETA',/,8X,
     *'2     P2 VS. THETA',/,8X,'3     NORMALIZED P1/P2 VS. THETA',
     */,8X,'4     EFFECTIVE BEAMWIDTH VS. THETA',/,8X,
     *'5     NUMBER OF REPLIES VS. THETA',/,8X,
     *'6     P1 VS. R(SLANT LENGTH)')
  115 FORMAT(' WHAT IS THE HEIGHT OF THE AIRCRAFT?')
C
C*****PLOT THE GRAPHS
C
       WRITE(7,105)
      CALL FREAD(7,'I:',NUMPLT)
      WRITE(7,110)
      DO 200 I=1,NUMPLT
   60 WRITE(7,106)
      CALL FREAD(7,'I:',N1)
      IF (N1 .LT.1 .OR. N1 .GT. 6 ) GO TO 80
      IF (N1 .EQ. 6) GO TO 150
      WRITE(7,107)
```

```
      Q=B
      CALL FREAD(7,'S:',Q,1)
      IF (Q .EQ. N) N1=N1+5
      IF (N1 .LE. 5) GO TO 75
      WRITE(7,108)
      Q=B
      CALL FREAD(7,'S:',Q,1)
      IF (Q .EQ. Y) GO TO 70
      NO=0
      GO TO 75
   70 NO=400
   75 GO TO (45,46,47,48,49,50,51,52,53,54),N1
   80 WRITE(7,109)
      GO TO 60
   45 CALL PLT(THETAD(1),P1LEVL(1),400,THETAD(1),P1NEW(1),400,THETAD(1),
     *P1FREE(1),400,XPRINT(1),YPRNT1(1),T1(1),T2(1),T3(1),1)
      GO TO 200
   46 CALL PLT(THETAD(1),P2LEVL(1),400,THETAD(1),P2NEW(1),400,THETAD(1),
     *P2FREE(1),400,XPRINT(1),YPRNT1(1),T1(1),T2(1),T3(1),1)
      GO TO 200
   47 CALL PLT(THETAD(1),P12LVL(1),400,THETAD(1),P1P2(1),400,0.0,0.0,0,
     *XPRINT(1),YPRNT2(1),T1(1),T2(1),T4(1),2)
      GO TO 200
   48 CALL PLT(THETAD(1),BEMLVL(1),400,THETAD(1),BEMNEW(1),400,0.0,0.0,
     *0,XPRINT(1),YPRNT3(1),T1(1),T2(1),T3(1),3)
      GO TO 200
   49 CALL PLT(THETAD(1),NUMLVL(1),400,THETAD(1),NUMNEW(1),400,0.0,0.0,
     *0,XPRINT(1),YPRNT4(1),T1(1),T2(1),T3(1),4)
      GO TO 200
   50 CALL PLT(THETAD(1),P1NEW(1),400,0.0,0.0,0,THETAD(1),P1FREE(1),NO,
     *XPRINT(1),YPRNT1(1),T1(1),T2(1),T3(1),1)
      GO TO 200
   51 CALL PLT(THETAD(1),P2NEW(1),400,0.0,0.0,0,THETAD(1),P2FREE(1),NO,
     *XPRINT(1),YPRNT1(1),T1(1),T2(1),T3(1),1)
      GO TO 200
   52 CALL PLT(THETAD(1),P1P2(1),400,0.0,0.0,0,0.0,0.0,0,XPRINT(1),
     *YPRNT2(1),T1(1),T2(1),T4(1),2)
      GO TO 200
   53 CALL PLT(THETAD(1),BEMNEW(1),400,0.0,0.0,0,0.0,0.0,0,XPRINT(1),
     *YPRNT3(1),T1(1),T2(1),T3(1),3)
      GO TO 200
   54 CALL PLT(THETAD(1),NUMNEW(1),400,0.0,0.0,0,0.0,0.0,0,XPRINT(1),
     *YPRNT4(1),T1(1),T2(1),T3(1),4)
      GO TO 200
  150 CALL PLT(R(1),P1(1),151,0.0,0.0,0,R(1),P1FRE(1),151,XPRNT1(1),
     *YPRNT1(1),T1(1),T2(1),T3(1),1)
  200 CONTINUE
      END
```

```
      SUBROUTINE PLT(X1,Y1,N1,X2,Y2,N2,X3,Y3,N3,XPRINT,YPRINT,T1,T2,T3,MM)
      DIMENSION X1(400),X2(400),X3(400),DY1(6),YMIN1(6)
      DIMENSION Y1(400),Y2(400),Y3(400)
      DIMENSION XPRINT(10),YPRINT(10),T1(10),T2(10),T3(10)
      CALL PLTXMX(10.0)
      CALL PSCALE(5.0,1.0,XMIN,DX,X1,N1,1,X2,N2,1,X3,N3,1)
      IF(MM.NE.2) GO TO 5
      CALL PSCALE(6.0,1.0,YMIN,DY,Y1,N1,1,Y2,N2,1,Y3,N3,1)
      YMIN1(2)=YMIN
    5 DY1(1)=8.0
      DY1(2)=5.0
      DY1(3)=1.0
      DY1(4)=8.0
      YMIN1(3)=0.0
      YMIN1(4)=0.0
      YMIN1(1)=-36.0
      CALL PLTOFS(XMIN,DX,YMIN1(MM),DY1(MM),3.0,3.0)
      CALL PAXIS(3.0,3.0,XPRINT,-30,5.0,0.0,XMIN,DX,1.0)
      CALL PAXIS(3.0,3.0,YPRINT,30,6.0,90.0,YMIN1(MM),DY1(MM),1.0)
      CALL PLTRFC
      CALL PLINE(X1,Y1,N1,1,0,0,1.0)
    1 IF (N2.EQ.0) GO TO 15
      CALL PDSHLN(X2,Y2,N2,1,0.1,1.0)



   15 IF(N3.EQ.0) GO TO 2
      CALL PLINE(X3,Y3,N3,1,0,0,1.0)
    2 CL=PSYMLN(0.15,30)
      CALL PSYMB(5.25-CL/2.,2.0,0.15,T1,0.0,40)
      CALL PSYMB(5.25-CL/2.,1.8,0.15,T2,0.0,40)
      CALL PSYMB(5.25-CL/2.,1.6,0.15,T3,0.0,40)
      CALL PLTEND
      RETURN
      END
```

APPENDIX C
REPORT OF INVENTIONS

A diligent review of the work performed under this contract has revealed no new innovation, discovery, improvement or invention.